

Duality symmetries and effective dynamics in disordered hopping models

Robert L. Jack

Department of Physics, University of Bath, Bath BA2 7AY, UK

Peter Sollich

King's College London, Department of Mathematics, London WC2R 2LS, UK

Abstract. We identify a duality transformation in one-dimensional hopping models that relates propagators in general disordered potentials linked by an up-down inversion of the energy landscape. This significantly generalises previous results for a duality between trap and barrier models. We use the resulting insights into the symmetries of these models to develop a real-space renormalisation scheme that can be implemented computationally and allows rather accurate prediction of propagation in these models. We also discuss the relation of this renormalisation scheme to earlier analytical treatments.

1. Introduction

The motion of particles in disordered environments is important in many contexts, from glass-forming liquids and colloids [1, 2], to biomolecules moving in the crowded environment of the cell [3], to electrical properties of disordered materials [4]. In this article, we discuss subdiffusive propagation in simple one-dimensional models. While the case of one-dimensional motion may seem simplistic, it is relevant for a variety of model systems: from early studies of electrical transport [4] to recently-defined models of glassy behaviour [5], and also to the motion of defects in disordered magnets, to disordered elastic chains and to networks of resistors and capacitors (see [6, 7, 8, 9] for reviews).

The results that we will present are based around a duality symmetry which relates pairs of discrete one-dimensional models. In a previous study [10], we showed that motion in apparently disparate models can be related exactly, at fixed disorder. Here we generalise those results to a much wider range of hopping models, by treating their master equations in a simple operator formalism. We also discuss how these results are related to earlier studies of disordered reaction-diffusion systems by Schütz and Mussawisade [11]. Based on the symmetries of the problem, we then introduce a real-space renormalisation scheme in the spirit of that of le Doussal, Monthus and Fisher [12]: our scheme is implemented computationally and allows rapid prediction of the propagation in these energy landscapes for fixed disorder, at low computational cost.

The central feature of the renormalisation scheme is that on a given time scale, we have a procedure for decomposing the system into effective trap and barrier regions. Particles within trap regions equilibrate there, while those in barrier regions decay into the effective traps. The duality symmetry relates trap and barrier regions of pairs of models, and demands that they be treated on an equal footing within the renormalisation scheme. In some sense, the renormalisation scheme is connected with the ideas of an energy landscape in these disordered systems [13], but we note that all properties of the energy landscape are here derived directly from the master operator of the stochastic dynamics. In this sense, our scheme allows the energy landscape to be derived from the dynamical rules of the system: this is the opposite of the usual situation in which thermodynamic properties are used to infer the routes by which dynamical processes take place. Thus, while our results are clearly restricted to a very simple class of models, it is natural to ask if they might be generalised to higher-dimensional energy landscapes.

The form of the paper is as follows: in Sec. 2 we define our models and give the duality relation between their master operators. The consequences of the duality relation for propagation in these models are discussed in Sec. 3. In Sec. 4 we explain our effective dynamics scheme; Sec. 5 contains numerical results for specific ensembles of disordered models; and Sec. 6 closes with a brief summary and some open questions.

2. Models and duality relations

We define a disordered one-dimensional hopping model in terms of rates for hops from site i to sites $i - 1$ and $i + 1$, which we denote by ℓ_i and r_i respectively. Let $p_i(t)$ be the probability that a particle occupies site i at time t : the master equation is then

$$\frac{\partial}{\partial t} p_i(t) = \ell_{i+1} p_{i+1}(t) + r_{i-1} p_{i-1}(t) - (\ell_i + r_i) p_i(t). \quad (1)$$

For concreteness, we consider a periodic chain of N sites, but we are primarily concerned with propagation of particles on infinite chains: that is, we consider the limit of large N before any limit of large time. In this limit, propagators will be independent of the choice of boundary conditions. We also discuss finite chains with reflecting and absorbing boundaries in section 2.1 below.

We use an operator notation where the ket $|i\rangle$ represents the state with the particle on site i , normalised so that $\langle i|j\rangle = \delta_{ij}$. Then, defining the state $|P(t)\rangle = \sum_i p_i(t)|i\rangle$, the master equation can be written as $\frac{\partial}{\partial t}|P(t)\rangle = W^{(1)}|P(t)\rangle$ with

$$W^{(1)} = \sum_{i=1}^N [\ell_i|i-1\rangle + r_i|i+1\rangle - (l_i + r_i)|i\rangle] \langle i| \quad (2)$$

$$= \sum_{i=1}^N (|i+1\rangle - |i\rangle)(r_i\langle i| - \ell_{i+1}\langle i+1|). \quad (3)$$

In this section, and wherever we consider systems with periodic boundaries, site $i = N + 1$ is equivalent to site 1 and site 0 is equivalent to site N . This allows terms to be rearranged as e.g. in going from (2) to (3) above.

We initially focus on an important special case: we assume that all rates are finite and that $\prod_i \ell_i = \prod_i r_i$. This ensures that all currents vanish in the long-time limit of the system. Under this assumption, we associate an energy with each site, measured *downwards* from an arbitrary baseline and determined through $\ell_{i+1}e^{E_{i+1}} = r_i e^{E_i}$. Then, the model respects detailed balance with respect to the distribution $p_i^{\text{eq}} = e^{E_i} / (\sum_r e^{E_r})$, where the sum runs over all sites. With this sign convention, a site with large positive E_i has a large Gibbs weight. The reason for this choice will become clear below.

We now discuss general duality relations between pairs of hopping models. To this end, we re-parameterise the transition rates ℓ_i and r_i by defining transition state energies $E_{i+\frac{1}{2}}$ associated with the links between sites:

$$\ell_i = e^{-(E_{i-\frac{1}{2}} + E_i)}, \quad r_i = e^{-(E_{i+\frac{1}{2}} + E_i)} \quad (4)$$

Note that site energies E_i and transition state energies $E_{i+\frac{1}{2}}$ are measured with respect to separate arbitrary baselines, so they do not necessarily have to be positive; but an interpretation in terms of activated hopping processes becomes problematic unless $E_i + E_{i\pm\frac{1}{2}} > 0$.

Two subclasses of these general hopping models have been studied quite extensively in the past [4, 6, 8, 10, 14, 15, 16, 17]. The first subclass is the (pure) trap model, which is the case $E_{i+\frac{1}{2}} = 0$ for all i , with the E_i being independent and identically distributed (i.i.d.); the second is the (pure) barrier model, which has $E_i = 0$ for all i , with the $E_{i+\frac{1}{2}}$ being i.i.d. A duality between pure trap and pure barrier models was discussed in [10], which we now generalise. The duality relation involves an inversion of the potential, which swaps the meaning of transition state energies and site energies: the various definitions are illustrated in Fig. 1. To present this relation, we define an alternative representation of the general hopping model, in which sites have indices $i + \frac{1}{2}$ (throughout this article, i is always an integer). The hopping rate from $i - \frac{1}{2}$ to $i + \frac{1}{2}$ is R_i and the rate for the reverse process is L_i . The master equation for this process has a similar representation in terms of state vectors

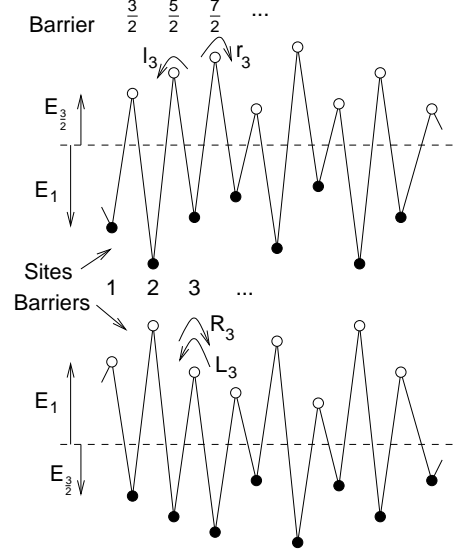


Figure 1. (Top) Illustration of an ‘energy landscape’, defined by supplementing the site energies E_i by transition state energies $E_{i+\frac{1}{2}}$. The rate for hopping from a site is related to the sum of the site energy (measured downwards as shown) and the adjacent transition state energy (measured upwards). (Bottom) On inversion of the potential, the transition state energies become energies of new sites with half-integer indices. Transition rates between these sites are controlled by the energies E_i which now have an interpretation as transition state energies.

$|i + \frac{1}{2}\rangle$, with a master operator

$$W^{(1/2)} = \sum_{i=1}^N (|i + \frac{1}{2}\rangle - |i - \frac{1}{2}\rangle) (R_i \langle i - \frac{1}{2}| - L_i \langle i + \frac{1}{2}|). \quad (5)$$

If we choose $R_i = r_i$ and $L_i = \ell_{i+1}$, then $W^{(1/2)}$ describes the same model as $W^{(1)}$, up to a simple relabelling of sites (site i in $W^{(1)}$ is mapped to site $i - \frac{1}{2}$ in $W^{(1/2)}$). To describe instead the inverted potential of Fig. 1, we choose

$$R_i = e^{-(E_i + E_{i-\frac{1}{2}})} = \ell_i, \quad L_i = e^{-(E_i + E_{i+\frac{1}{2}})} = r_i \quad (6)$$

With these definitions, the duality relation takes a simple form: we define operators

$$S = \sum_{i=1}^N (|i + 1\rangle - |i\rangle) \langle i + \frac{1}{2}| e^{-E_{i+\frac{1}{2}}} \quad (7)$$

$$= \sum_{i=1}^N |i\rangle \left(e^{-E_{i-\frac{1}{2}}} \langle i - \frac{1}{2}| - e^{-E_{i+\frac{1}{2}}} \langle i + \frac{1}{2}| \right) \quad (8)$$

and

$$\bar{S} = \sum_{i=1}^N (|i + \frac{1}{2}\rangle - |i - \frac{1}{2}\rangle) \langle i| e^{-E_i} \quad (9)$$

$$= \sum_{i=1}^N |i + \frac{1}{2}\rangle (\langle i|e^{-E_i} - \langle i+1|e^{-E_{i+1}}). \quad (10)$$

Hence, by combining the first expression (7) for S with the second expression (10) for \bar{S} , and *vice versa*, one verifies that

$$W^{(1)} = S\bar{S}, \quad W^{(1/2)} = \bar{S}S. \quad (11)$$

It follows that

$$\bar{S}W^{(1)} = W^{(1/2)}\bar{S}, \quad (12)$$

and that

$$W^{(1)}S = SW^{(1/2)}. \quad (13)$$

These two relations express the key duality between the two master operators from which all our other results are derived. They imply, for example, that $W^{(1)}$ and $W^{(1/2)}$ have the same spectrum of eigenvalues: if $|\psi\rangle$ is a right eigenvector of $W^{(1/2)}$ then $S|\psi\rangle$ is a right eigenvector of $W^{(1)}$ with the same eigenvalue. The exception is the singular case where $S|\psi\rangle = 0$, which can happen only when the eigenvalue is zero. An analogous argument can be made in the other direction, showing overall that the nonzero eigenvalues and associated eigenvectors of $W^{(1)}$ and $W^{(1/2)}$ are in one-to-one correspondence with each other.

In fact, the structure of (11) occurs in the context of supersymmetric field theories (for a discussion of supersymmetry in the language of operators, applied to energy landscapes, see [18]; for a more general introduction, see [19]). These hopping models are very simple examples of supersymmetric partners: the spaces $\{|i\rangle\}$ and $\{|i + \frac{1}{2}\rangle\}$ can be interpreted as zero- and one-fermion subspaces of a generalised superspace. Acting to the right, the operator S annihilates all elements of $\{|i\rangle\}$ and \bar{S} annihilates all elements of $\{|i + \frac{1}{2}\rangle\}$ so $S^2 = \bar{S}^2 = 0$: these operators are the supercharges of the theory. We can then write $W^{(1)} + W^{(1/2)} = S\bar{S} + \bar{S}S$ which allows us to identify the two models as supersymmetric partners.

It is also instructive to consider the continuum limit of our lattice model. Assume that the lattice spacing is a , so that the position of site i is $x_i = ia$. We define continuous functions $V_1(x)$ and $V_{1/2}(x)$ and take $E_i = V_1(x_i)$ and $E_{i+\frac{1}{2}} = V_{1/2}(x_{i+\frac{1}{2}})$. Within the continuum limit, we represent the superspace explicitly, using a basis $|x, n\rangle$, where x is the position and $n = 0, 1$ distinguishes the zero- and one-fermion subspaces. That is, taking fermionic operators c, c^\dagger with $c^2 = (c^\dagger)^2 = 0$ and $cc^\dagger + c^\dagger c = 1$, we take $c|x, 0\rangle = 0$ and $|x, 1\rangle = c^\dagger|x, 0\rangle$. To make contact with the basis used for the lattice model, we identify $|i\rangle$ with $|x_i, 0\rangle$ and $|i + \frac{1}{2}\rangle$ with $|x_i, 1\rangle$. If we then divide S and \bar{S} by a and take the lattice spacing to zero, we arrive at

$$S = c \frac{d}{dx} e^{-V_{1/2}(x)}, \quad \bar{S} = c^\dagger \frac{d}{dx} e^{-V_1(x)} \quad (14)$$

The master (or Fokker-Planck) operators follow as

$$\begin{aligned} W^{(1)} &= S\bar{S} = cc^\dagger \frac{d}{dx} e^{-V_{1/2}(x)} \frac{d}{dx} e^{-V_1(x)}, \\ W^{(1/2)} &= \bar{S}S = c^\dagger c \frac{d}{dx} e^{-V_1(x)} \frac{d}{dx} e^{-V_{1/2}(x)} \end{aligned} \quad (15)$$

This makes it obvious that the duality just swaps the trap and barrier parts of the potential, i.e. inverts the energy landscape. In the case without thermal activation,

which corresponds to $V_{1/2} = -V_1 = V$, the duality reduces to the standard one for diffusion in the potentials V and $-V$. One part of this duality was used recently in [20] to map boundary-driven steady states with current to current-free equilibrium states. Briefly, if $P(x)$ is a steady state probability distribution of $W^{(1)}$ in the presence of a boundary field so that $W^{(1)}|P(x), 0\rangle = 0$, then $|\tilde{P}(x), 1\rangle = \bar{S}|P(x), 0\rangle$ obeys $S|\tilde{P}(x), 1\rangle = 0$. Thus, $|\tilde{P}(x), 1\rangle$ is a steady state of $W^{(1/2)}$, but the current in this state is $-e^V(d/dx)e^{-V}|\tilde{P}(x), 1\rangle = -e^V c^\dagger S|\tilde{P}(x), 1\rangle = 0$. The same approach also works on the lattice, and indeed the rate transformation (182) in Ref. [20] is the same as our (6).

The total master operator combining the dynamics in the zero and one-fermion spaces can be made Hermitian by a standard similarity transformation: with $X = cc^\dagger e^{\frac{1}{2}V_1(x)} + c^\dagger c e^{\frac{1}{2}V_{1/2}(x)}$ one has

$$\begin{aligned}
 H &= X^{-1}(W^{(1)} + W^{(1/2)})X \\
 &= cc^\dagger e^{-\frac{1}{2}V_1(x)} \frac{d}{dx} e^{-V_{1/2}(x)} \frac{d}{dx} e^{-\frac{1}{2}V_1(x)} + c^\dagger c e^{-\frac{1}{2}V_{1/2}(x)} \frac{d}{dx} e^{-V_1(x)} \frac{d}{dx} e^{-\frac{1}{2}V_{1/2}(x)} \quad (16)
 \end{aligned}$$

Using $cc^\dagger = 1 - c^\dagger c$ to extract the extra contribution from the one-fermion subspace, one can simplify this to

$$\begin{aligned}
 H &= e^{-\frac{1}{2}V_1(x)} \frac{d}{dx} e^{-V_{1/2}(x)} \frac{d}{dx} e^{-\frac{1}{2}V_1(x)} \\
 &\quad - c^\dagger c e^{-V_1(x) - V_{1/2}(x)} \left[\frac{1}{4}(V_1'(x)^2 - V_{1/2}'(x)^2) - \frac{1}{2}(V_1''(x) - V_{1/2}''(x)) \right] \quad (17)
 \end{aligned}$$

For the ‘standard’ case with uniform diffusion constant $V_{1/2} = -V_1 = V$, the one-fermion term simplifies to $-c^\dagger c V''(x)$ and this is exactly the term that was used e.g. in [18, 19] to construct dynamics that (in one dimension, and in the one-fermion subspace) converges to maxima rather than minima of the potential.

2.1. Choice of boundary conditions

In the previous section, we discussed systems with detailed balance and periodic boundaries. We now discuss how the duality relation applies on finite chains with reflecting or absorbing boundaries. We note in passing that some of these relations may be generalised both to boundary-driven models and to those with a finite bias acting in the bulk [21]. However, for this work, we restrict ourselves to models without a steady-state current.

In the case of periodic boundary conditions, the derivation of our duality relations required that the rates satisfy the global constraint $\prod_i \ell_i = \prod_i r_i$, in order to guarantee detailed balance. An alternative that avoids this constraint is to use finite chains with reflecting or absorbing boundary conditions. These can be obtained by allowing zero rates in the periodic system. For a system with reflecting boundaries, we take $\ell_1 = r_N = 0$ in $W^{(1)}$. In the notation of energies, we set formally $e^{-E_{\frac{1}{2}}} = 0$: sites 1 and N are then reflecting boundaries because they are separated by an infinite barrier. This has no effect on the equilibrium steady state, which now satisfies detailed balance whatever our choice for the remaining nonzero rates. The duality transformation carries through as before, resulting in a system with $L_N = R_1 = 0$. In this system there are no transitions out of site $\frac{1}{2}$, which is therefore absorbing. The duality thus relates models with reflecting and absorbing boundaries, and as before these models share the same eigenvalues and their eigenvectors (for nonzero eigenvalues) are related

through the operators S and \overline{S} . Note that for $W^{(1/2)}$, the steady state that is reached in the long-time limit has the particle fully localised on the absorbing site $\frac{1}{2}$. Detailed balance still holds, with e.g. the propagators obeying (24) below; the balance of transitions in the steady state is trivial because there are no transitions taking place at all.

One can go further by distinguishing whether the absorbing site in $W^{(1/2)}$ is reached from the left (from site $\frac{3}{2}$) or from the right (from site $N - \frac{1}{2}$), and accordingly split the absorbing site into two sites $\frac{1}{2}$ and $N + \frac{1}{2}$. The duality relation to the system $W^{(1)}$ with two reflecting boundaries then holds as before. The only difference is that, because the system now has two absorbing sites, the master operator has two zero eigenvalues. The two corresponding right eigenvectors are localised on the absorbing sites, while the elements of the left eigenvectors give the probabilities that a particle initially on a given site will end up on either one of the absorbing sites (this will be discussed further in later sections).

Finally, one may also take an operator $W^{(1)}$ with one reflecting boundary and an absorbing site at the other boundary: this can be done by setting $e^{-E\frac{1}{2}} = 0$ and $e^{-EN} = 0$, so that $\ell_1 = \ell_N = r_N = 0$. In the dual model of this system, $R_1 = R_N = L_N = 0$, so that the reflecting boundary at site 1 maps to an absorbing boundary at site $\frac{1}{2}$ and *vice versa* for sites N and $N - \frac{1}{2}$.

2.2. Alternative formulation, and generalised duality

So far, our results apply to models in which the steady state has zero current (that is, periodic chains with global detailed balance, and chains with reflecting or absorbing boundaries). However, there is a slightly modified duality relation that holds even for periodic chains without detailed balance, where the steady state has finite current. Instead of factorising $W^{(1)} = S\overline{S}$ as in (11), one may instead write

$$W^{(1)} = -DJ \quad (18)$$

with $D = \sum_i (|i\rangle - |i+1\rangle)\langle i + \frac{1}{2}|$ and $J = \sum_i |i + \frac{1}{2}\rangle (r_i \langle i| - \ell_{i+1} \langle i+1|)$. [In the continuum limit, one has $W^{(1)} = -\frac{d}{dx}J$ where $J = -e^{-V_{1/2}(x)} \frac{d}{dx} e^{-V_1(x)}$ is the probability current operator, so the master (Fokker-Planck) equation has the form $\partial_t P = -\nabla(JP)$ as usual, where JP is the probability current, which is linear in P .

With these definitions, one may verify that

$$W^{(1/2)} = -(JD)^\dagger \quad (19)$$

or equivalently that

$$W^{(1)}D = -DJD = D(W^{(1/2)})^\dagger. \quad (20)$$

If detailed balance holds, the relation $\langle i + \frac{1}{2}|W^{(1/2)}|j + \frac{1}{2}\rangle e^{E_{j+\frac{1}{2}}} = \langle j + \frac{1}{2}|W^{(1/2)}|i + \frac{1}{2}\rangle e^{E_{i+\frac{1}{2}}}$ may be combined with (19) to recover (13). (One way is to define $E = \sum_i |i + \frac{1}{2}\rangle \langle i + \frac{1}{2}| e^{E_{i+\frac{1}{2}}}$ and to note that $D = -SE$, $J = E^{-1}\overline{S}$, and by detailed balance $W^{(1/2)} = E(W^{(1/2)})^\dagger E^{-1} = -EJDE^{-1} = \overline{S}S$.)

We also note that the operator D may not be inverted, since $D \sum_i |i + \frac{1}{2}\rangle = 0$. However, if one considers for example a periodic chain of N sites with an absorbing site 1 and a reflecting barrier $\frac{1}{2}$, so that $r_1 = \ell_1 = r_N = 0$, then one may write $W^{(1)} = -D'J$ and $W^{(1/2)} = -(JD')^\dagger$ with $D' = D + |1\rangle\langle \frac{1}{2}|$. In that case, it may be verified that the inverse of D' does exist, and the duality transformation becomes

$$(D')^{-1}W^{(1)}D' = (W^{(1/2)})^\dagger \quad (21)$$

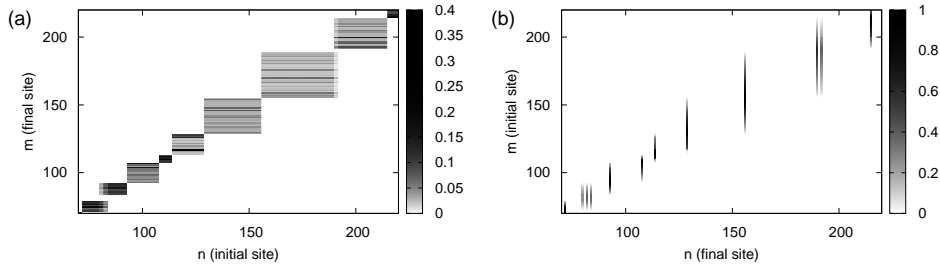


Figure 2. Plots of Green's functions that illustrate the duality relation between the propagators. The plots were generated using the effective dynamics scheme described in section 4, but (26) applies to propagation under the effective dynamics as well as to propagation with real dynamics. (Left) Propagator $G_{m,n}$, describing motion from site n to site m in a model of mixed trap-barrier type with $\mu_B = 3$ and $\mu_T = 0.5$ (see Sec. 5.1 for definitions). The 'squares' represent 'trap regions' within which the particle is locally equilibrated. The structure within the trap depends on the final site energies. These energies are randomly distributed, so that sites with low energy $-E_i$ give rise to dark 'stripes'. However, local equilibration within the trap means that the propagator depends only weakly on the initial site n for all the n within a single trap. (Right) Propagator $G_{n,m}$ in the dual model of that shown on the left: note that m is now the initial site and n the final site. The probability for the final position is localised on a few deep 'trap' sites. Eq. (26) states that for given values of m and n , the gradient of the right plot in the vertical (m)-direction is equal to the gradient of the left plot in the horizontal (n)-direction.

We note that the transformation operators D and D' do not depend on the disordered rates r_i and ℓ_i . An invertible transformation that is independent of disorder was used by Schütz and Mussawisade [11] to study a reaction-diffusion model in a similar disordered environment. The duality transformation (enantiodromy) \mathcal{D} used in [11] is related to the transformation D' , and can be used to prove some of the relations for propagators that we discuss in the next section. However, analysis of the reaction-diffusion model is much more complex than the single particle system considered here. In the following, we restrict our analysis to the single-particle case, explaining which results may be obtained by alternative means.

3. Propagators

We now consider the propagators of these hopping models. For convenience, we first consider periodic boundaries in the case where detailed balance holds. Generalisations to reflecting/absorbing boundaries are straightforward using the approach discussed above (Sec. 2.1). For the model $W^{(1)}$, we define the propagator $G_{n,m}^{(1)}(t)$ as the probability that the particle is on site n , given that it was on site m a time t earlier:

$$G_{n,m}^{(1)}(t) = \langle n | e^{W^{(1)}t} | m \rangle \quad (22)$$

Similarly, for the model $W^{(1/2)}$, we define

$$G_{n+\frac{1}{2},m+\frac{1}{2}}^{(1/2)}(t) = \langle n + \frac{1}{2} | e^{W^{(1/2)}t} | m + \frac{1}{2} \rangle \quad (23)$$

Detailed balance holds for both models so we have, bearing in mind our sign convention for energies, $G_{n,m}^{(1)}(t)e^{E_m} = G_{m,n}^{(1)}(t)e^{E_n}$ or

$$e^{-E_n}G_{n,m}^{(1)}(t) = e^{-E_m}G_{m,n}^{(1)}(t), \quad (24)$$

with a similar relation for $G^{(1/2)}$. We now appeal to the duality relation $\overline{S}W^{(1)} = W^{(1/2)}\overline{S}$ to obtain $\langle n + \frac{1}{2} | \overline{S} e^{W^{(1)}t} | m \rangle = \langle n + \frac{1}{2} | e^{W^{(1/2)}t} \overline{S} | m \rangle$. Using the explicit form of \overline{S} , we arrive at

$$e^{-E_n}G_{n,m}^{(1)}(t) - e^{-E_{n+1}}G_{n+1,m}^{(1)}(t) = \left[G_{n+\frac{1}{2},m+\frac{1}{2}}^{(1/2)}(t) - G_{n+\frac{1}{2},m-\frac{1}{2}}^{(1/2)}(t) \right] e^{-E_m}, \quad (25)$$

from which detailed balance for $W^{(1)}$ implies

$$G_{m,n}^{(1)}(t) - G_{m,n+1}^{(1)}(t) = G_{n+\frac{1}{2},m+\frac{1}{2}}^{(1/2)}(t) - G_{n+\frac{1}{2},m-\frac{1}{2}}^{(1/2)}(t). \quad (26)$$

This result generalises Eq. (5) of Ref. [10]. Equation (26) may also be proved directly using the relation (20). Hence, this relation between propagators applies on periodic chains, regardless of whether detailed balance holds. It holds for all times, including cases where the limit of large time is taken at fixed system size.

Two comments are in order here. Firstly, a relation similar to (26) was proven for propagators in the reaction-diffusion model of [11]. That model has pair annihilation, so we consider an initial state with two well-separated particles. If one then takes the limit $N \rightarrow \infty$ at fixed time, one arrives at two independently propagating particles which can be shown to satisfy (26). However, the mapping of [11] cannot be used to prove (26) for large times and periodic chains of fixed length: in that case, it would be natural to use an initial state with exactly one particle but the mapping then breaks down (except for specific cases where the periodic chain is broken into segments by absorbing sites and reflecting barriers). Secondly, for the specific case where the E_i are chosen freely but $E_{i+\frac{1}{2}} = 0$ for all i , the relation (26) was given in Ref. [10], but it is also implicit in Ref. [22]. (In the notation there, it reads $f(q)\hat{\Gamma}_{qq'}^B(z) = \hat{\Gamma}_{qq'}^T(z)f(q')$ and can be derived by inserting Eqs. (2.15) and (2.16) into (2.19) of Ref. [22] and expanding appropriately.)

The equality (26) relates differences with respect to the initial site of propagators in the two hopping models. If the propagator for one model is known, the other can be calculated by successive application of this equation. An illustration of this relation is shown in Fig. 2. We also note that (26) is symmetric between the two master operators: any set of transition rates can be interpreted either as a model of type $W^{(1)}$ or as a model of type $W^{(1/2)}$. To reinforce this symmetry, we note that the relation $\langle n | S e^{W^{(1/2)}t} | m - \frac{1}{2} \rangle = \langle n | e^{W^{(1)}t} S | m - \frac{1}{2} \rangle$ implies that

$$e^{-E_{n-\frac{1}{2}}}G_{n-\frac{1}{2},m-\frac{1}{2}}^{(1/2)}(t) - e^{-E_{n+\frac{1}{2}}}G_{n+\frac{1}{2},m-\frac{1}{2}}^{(1/2)}(t) = \left[G_{n,m}^{(1)}(t) - G_{n,m-1}^{(1)}(t) \right] e^{-E_{m-\frac{1}{2}}} \quad (27)$$

which is the same relation as (25), but with the original model $W^{(1)}$ expressed in the form $W^{(1/2)}$ and *vice versa*.

The simple form of (26) means that we can take the disorder average. As long as the disorder is translationally invariant, e.g. if the transition state energies $\{E_{i+\frac{1}{2}}\}$ and site energies $\{E_i\}$ are taken from two (possibly different) translationally invariant distributions, the disorder-averaged propagators $\overline{G}_{n,m}(t)$ will depend only on $k = n - m$. Defining then $\Delta_k = \overline{G}_k^{(1)}(t) - \overline{G}_{-k}^{(1/2)}(t)$, the relation (26) becomes $\Delta_{-k} = \Delta_{-k-1}$. Thus, Δ_k is a constant; but $\sum_k \overline{G}_k^{(1)}(t) = 1$ and similarly for $\overline{G}_k^{(1/2)}(t)$,

so $\sum_k \Delta_k = 0$ and the constant has to vanish. One concludes that $\overline{G}_k^{(1)}(t) = \overline{G}_{-k}^{(1/2)}(t)$. Re-instating the notation with separate initial and finite site labels, we have

$$\overline{G}_{m,n}^{(1)}(t) = \overline{G}_{n,m}^{(1/2)}(t) = \overline{G}_{m,n}^{(1/2)}(t) \quad (28)$$

where the last equality follows from left-right symmetry. Remarkably, then, the disorder-averaged propagators of the dual models are equal on all scales of length and time. Again, this generalises our earlier statement [10] relating average propagators in pure trap and barrier models. A similar result applies for disorder distributions which break left-right symmetry, as long as they remain translationally invariant. Take for example a model described by $W^{(1)}$ with site and barrier energies from a translationally invariant distribution, and then modify the rates according to a site-independent prescription, so that the left-going and right-going rates acquire different distributions. With periodic boundary conditions, translation invariance again holds and we obtain by the same arguments as above

$$\overline{G}_{m,n}^{(1)}(t) = \overline{G}_{n,m}^{(1/2)}(t), \quad (29)$$

with both sides again depending only on the difference $k = n - m$. The same result applies on long chains with reflecting boundaries, as long as we are far away from these boundaries so that translation invariance is not broken.

4. Effective dynamics scheme

Several effective dynamics and renormalisation schemes have been proposed to approximate propagators for motion in random potentials [12, 14, 17, 23]. The most notable success in this area is the work of le Doussal, Monthus and Fisher [12], which we refer to as DMF. They considered the Sinai model [24], in which the r_i and ℓ_i are independently and identically distributed, so that the site energies E_i follow a random walk in real space. For long time scales in that model, DMF found a renormalisation group (RG) scheme that can be implemented analytically and gives exact results for a variety of observables.

Later, Monthus [17] applied a related scheme to the pure trap model, in which $\ell_i = r_i$ and these rates are independently and identically distributed with a power-law distribution $P(r_i) \propto r_i^{(1/\mu)-1}$. We refer to this scheme as Mon03: it can be treated analytically and its predictions are exact in the limit of large μ (our notation follows that of [10]: to arrive at the notation of [17], replace μ by $\frac{1}{\mu}$). More recently, Monthus and Garel (MG) derived a general RG scheme [23] that is not restricted to one dimension nor to single-particle systems. Like the schemes of Refs. [12, 17], the MG scheme is effective when disorder is the dominant source of fluctuations. Finally, we recently [10] introduced a modified scheme for pure trap and barrier models that respects the duality symmetry (26) but requires a computational implementation. This prescription accounts for effects that were neglected in previous schemes, and reduces to the Mon03 scheme in the limits in which that method is exact.

Here, we generalise the scheme of [10] to general disordered potentials (in one dimension). We arrive at a method that encompasses the DMF and Mon03 methods in the limits when they are exact, and is also consistent with the duality relation (26). Our method also shares features with that of MG, but it respects the duality symmetries discussed above, while the MG scheme does not. We describe the application of this scheme to models parameterised in the form of $W^{(1)}$, with site

energies E_i and transition state energies $E_{i+\frac{1}{2}}$. For notational convenience, we simply denote these master operators by W from now on.

4.1. Definition of the effective dynamics scheme

The idea of the effective dynamics scheme is to describe motion on long time scales in terms of a coarse-grained set of co-ordinates in which the system evolves slowly. We have developed two versions of the scheme: in the main text we describe the more physical and intuitive version that also gives the most accurate description of motion in the system. We discuss the justifications of our scheme in later sections (Appendix A and Sec. 5): in particular, the second version of the scheme can be justified more formally, and it gives similar results, but with larger errors for finite μ .

The scheme is parameterised by a time scale Γ^{-1} . On that time scale, we partition the 1d chain into effective trap and effective barrier regions. The coarse-grained slow co-ordinates are the occupancies of the effective traps:

$$p_\alpha(t) = \sum_{i=a_\alpha}^{b_\alpha} p_i(t). \quad (30)$$

We continue to use Roman indices i, j, \dots for the original site labels of the model, while Greek indices α, β, \dots label the slow co-ordinates. Thus, a_α and b_α are the leftmost and rightmost sites within effective trap α . The traps form an ordered set along the chain, so we have $b_{\alpha-1} < a_\alpha \leq b_\alpha < a_{\alpha+1}$. We refer to the regions between these effective traps as effective barriers.

For a given value of Γ , the effective dynamics scheme gives (i) an approximation for the propagator $G_{mn}(\Gamma^{-1})$ and (ii) an approximate equation of motion for the slow co-ordinates, valid for times $t > \Gamma^{-1}$. In addition, the scheme specifies (iii) how the set of effective traps evolves as Γ is decreased towards zero.

Physically, the idea is that motion within effective traps is fast, while motion between traps is slow. Assuming equilibration within effective traps, we have for sites within an effective trap region,

$$G_{ji}(\Gamma^{-1}) \simeq e^{E_j - F_\alpha}, \quad a_\alpha \leq i, j \leq b_\alpha \quad (31)$$

where we identify the free energy of effective trap α :

$$e^{F_\alpha} = \sum_{i=a_\alpha}^{b_\alpha} e^{E_i} \quad (32)$$

If site i is between traps $\alpha - 1$ and α , that is $b_{\alpha-1} < i < a_\alpha$, then it may relax into either trap before equilibrating there, and we have

$$G_{ji}(\Gamma^{-1}) \simeq \begin{cases} (1 - v_i^{(\alpha-\frac{1}{2})})e^{E_j - F_{\alpha-1}}, & a_{\alpha-1} \leq j \leq b_{\alpha-1} \\ v_i^{(\alpha-\frac{1}{2})}e^{E_j - F_\alpha}, & a_\alpha \leq j \leq b_\alpha \end{cases} \quad (33)$$

where $v_i^{(\alpha-\frac{1}{2})}$ is the probability that a particle initially on a site i between traps $\alpha - 1$ and α relaxes first into trap α . These probabilities can be obtained by considering propagation on a chain with absorbing sites $b_{\alpha-1}$ and a_α , and calculating the probability of absorption into each of these sites for a given initial site i . The result is

$$v_i^{(\alpha-\frac{1}{2})} = e^{-F_{\alpha-\frac{1}{2}}} \sum_{j=b_{\alpha-1}}^{i-1} e^{E_{j+\frac{1}{2}}} \quad (34)$$

with

$$e^{F_{\alpha-\frac{1}{2}}} = \sum_{j=b_{\alpha-1}}^{a_{\alpha}-1} e^{E_{j+\frac{1}{2}}}. \quad (35)$$

This completes point (i) above. Turning to point (ii), the equations of motion for the slow degrees of freedom are

$$\partial_t p_{\alpha}(t) = \ell_{\alpha+1} p_{\alpha+1}(t) + r_{\alpha-1} p_{\alpha-1}(t) - (\ell_{\alpha} + r_{\alpha}) p_{\alpha}(t) \quad (36)$$

with

$$r_{\alpha} = e^{-F_{\alpha}-F_{\alpha+\frac{1}{2}}}, \quad \ell_{\alpha} = e^{-F_{\alpha}-F_{\alpha-\frac{1}{2}}} \quad (37)$$

That is, hopping takes place only between nearest neighbours, and the rates are given by the free energies of the effective traps F_{α} and ‘transition state free energies’ $F_{\alpha+\frac{1}{2}}$.

It remains to discuss point (iii) above: how the set of effective traps depends on the time scale Γ . Initially each effective trap contains a single site i , and each effective barrier a single transition site $i + \frac{1}{2}$. Each stage of our effective dynamics begins by calculating rates for motion from trap α : we calculate a renormalised rate ρ_{α} associated with the rate r_{α} , i.e. with leaving the trap to the right:

$$\rho_{\alpha} = \frac{1}{2}(r_{\alpha} + \ell_{\alpha} + \ell_{\alpha+1}) + \frac{1}{2}\sqrt{r_{\alpha}^2 + 2r_{\alpha}(\ell_{\alpha} + \ell_{\alpha+1}) + (\ell_{\alpha} - \ell_{\alpha+1})^2}. \quad (38)$$

and similarly for motion to the left

$$\lambda_{\alpha} = \frac{1}{2}(\ell_{\alpha} + r_{\alpha} + r_{\alpha-1}) + \frac{1}{2}\sqrt{\ell_{\alpha}^2 + 2\ell_{\alpha}(r_{\alpha} + r_{\alpha-1}) + (r_{\alpha} - r_{\alpha-1})^2}, \quad (39)$$

Notice that ρ_{α} is symmetric in ℓ_{α} and $\ell_{\alpha+1}$. In a (renormalised) landscape similar to that for pure traps, ℓ_{α} would be comparable to r_{α} and so $\rho_{\alpha} \approx r_{\alpha} + \ell_{\alpha}$ if the other rate ($\ell_{\alpha+1}$) is small. Conversely, in a landscape resembling pure barriers, one would have $\ell_{\alpha+1}$ of the same order as r_{α} and so to leading order $\rho_{\alpha} \approx r_{\alpha} + \ell_{\alpha+1}$. The expressions (38,39) cover both of these limits but extend them to general landscapes.

Having calculated the ρ_{α} and λ_{α} , we select the largest of these rates across all traps, and update Γ to this largest rate. At this point, several cases arise, which are illustrated in the following section, with reference to the example landscape in Fig. 3. Here we give the rules: Supposing that the largest rate is ρ_{α} , we now remove trap α . We make a case distinction, depending on whether the local landscape is nearer to the pure trap or the pure barrier case, as in the discussion of the rate-dependence of ρ_{α} above. If $\ell_{\alpha+1} > \ell_{\alpha}$ we combine trap α into trap $\alpha + 1$, leading to a new effective trap containing sites $a_{\alpha} \dots b_{\alpha+1}$. Barrier region $\alpha + \frac{1}{2}$ is removed. Conversely, if $\ell_{\alpha+1} < \ell_{\alpha}$, we remove trap α from the list of slow co-ordinates: this amounts to combining barrier regions $\alpha \pm \frac{1}{2}$. For the case where the largest renormalised rate is λ_{α} , associated with motion to the left, the rules are similar, in accordance with left-right symmetry: if $r_{\alpha-1} > r_{\alpha}$ we combine traps $\alpha - 1$ and α ; otherwise we remove trap α which amounts to combining the two barrier regions $\alpha \pm \frac{1}{2}$.

Having combined the appropriate traps or barriers, we finally recalculate the free energies F_{α} and $F_{\alpha+\frac{1}{2}}$ that are affected by the change, and hence obtain new hopping rates r_{α} and ℓ_{α} , and new renormalised rates ρ_{α} and λ_{α} . From here on the process is iterated, i.e. we find the largest rate among the $\{\rho_{\alpha}, \lambda_{\alpha}\}$, update Γ , and merge the appropriate traps or barriers.

For any given Γ , we can therefore calculate the approximate propagator and the equation of motion for the slow degrees of freedom. We emphasise that while we have

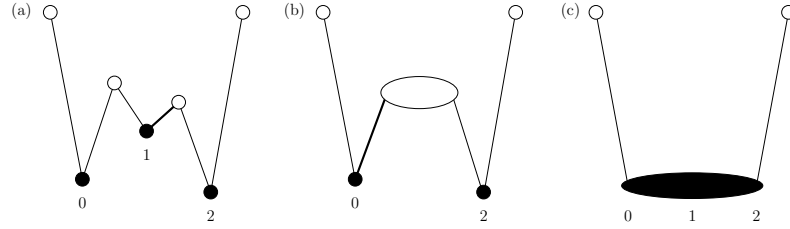


Figure 3. Illustration of the RG scheme introduced in this paper, discussed in the main text and in Appendix A. As in Fig. 1, sites are shown with closed circles and transition states with open circles. However, we now introduce effective trap regions, represented by filled ovals, and effective barrier regions, represented by open ovals. (a) Energy landscape for a hopping model with rates satisfying (40). The fastest rate r_1 is associated with the energy difference $E_1 + E_{\frac{3}{2}}$: the link associated with this rate is emphasised by a bold line. (b) Energy landscape obtained after one stage of renormalisation, with slow degrees of freedom $\{\dots, p_0(t), p_2(t), \dots\}$. The transition states $\frac{1}{2}$ and $\frac{3}{2}$ and site 1 have been incorporated into a composite transition state, which we refer to as an effective barrier region. Within the effective dynamics, a particle initially on site 1 relaxes either to site 0 or site 2, according to (33). The link associated with the largest rate in the renormalised master operator is again emphasised. (c) Energy landscape after the second stage of renormalisation, with slow degrees of freedom $\{\dots, p_0(t) + p_1(t) + p_2(t), \dots\}$. The two effective traps on sites 0 and 2 have been combined into a single effective trap. Within the effective dynamics, particles initially on any of these sites relax to an equilibrium distribution over sites 0, 1, 2.

defined rates $r_\alpha, \ell_\alpha, \lambda_\alpha, \rho_\alpha$, free energies $F_\alpha, F_{\alpha+\frac{1}{2}}$ and parameters $a_\alpha, b_\alpha, v_i^{(\alpha-\frac{1}{2})}$, all of these quantities are fixed if we specify the set of slow co-ordinates (parameterised in terms of the a_α and b_α), together with the full set of bare energies $E_i, E_{i+\frac{1}{2}}$. We discuss below how the progress of the scheme can be written in terms of a Γ -dependent projection operator, using the notation of Sec. 2. However, we first give an illustrative example of the effective dynamics in action.

4.2. Example of effective dynamics and comparison with DMF scheme

We illustrate the effective dynamics using the example landscape shown in Fig. 3, concentrating on sites 0, 1, 2 of a long chain. Consistent with Fig. 3a, we choose the rates to lie in three well-separated sectors:

$$r_1, \ell_1 \gg r_0, \ell_2 \gg \ell_0, r_2. \quad (40)$$

For concreteness we also take $r_1 > \ell_1$ (i.e. $E_{\frac{1}{2}} > E_{\frac{3}{2}}$), $\ell_2 > r_0$ and $E_2 > E_0$.

At the initial stage of the dynamics, sites 0, 1, 2 each constitute an effective trap: the effective equation of motion (36) coincides with the original master equation (1) and the relevant degrees of freedom are simply the original site occupancies $\{\dots, p_0(t), p_1(t), p_2(t), \dots\}$ where the (...) indicate that we are concentrating on part of a large chain. Taking the original rates r_i and ℓ_i , we evaluate the parameters ρ_α and λ_α , and the largest of these is $\rho_1 = r_1 + \ell_1 + \ell_2 + \frac{1}{2}\sqrt{r_1^2 + 2r_1(\ell_1 + \ell_2) + (\ell_1 - \ell_2)^2}$. (To leading order in the largest rates r_1 and ℓ_1 , $\rho_1 = \lambda_1 = r_1 + \ell_1$; but the correction from ℓ_2 can then be shown to make $\rho_1 > \lambda_1$.) Thus, the first step of the effective dynamics occurs as Γ is decreased through ρ_1 . From (40), we have $\ell_2 < \ell_1$, so the rules state that we remove the trap on site 1. Physically, the idea is that the transition state

energies $E_{\frac{1}{2}}$ and $E_{\frac{3}{2}}$ are similar to each other, so they are combined into an effective barrier. On the other hand, the particle spends very little time on site 1, compared to sites 0 and 2, so the co-ordinate $p_1(t)$ relaxes quickly to a small value and is no longer a relevant (slow) co-ordinate.

The remaining slow co-ordinates are therefore $\{\dots, p_0(t), p_2(t), \dots\}$, and the energy landscape on this time scale is shown in Fig. 3b. From (36), the equations of motion for these two co-ordinates at this stage are

$$\begin{aligned}\partial_t p_0(t) &= r_{-1}p_{-1}(t) + \ell'_2 p_2(t) - (r'_0 + \ell_0)p_0(t) \\ \partial_t p_2(t) &= r'_0 p_0(t) + \ell_3 p_3(t) - (r_2 + \ell'_2)p_2(t)\end{aligned}\quad (41)$$

where the unprimed rates r_i and ℓ_i are the original hopping rates among the sites of the model, but two new rates have appeared: $r'_0 = e^{-E_0 - F}$ and $\ell'_2 = e^{-E_2 - F}$. Here $e^F \equiv e^{E_{\frac{1}{2}}} + e^{E_{\frac{3}{2}}}$, and F is the ‘transition state free energy’ for the effective barrier region between sites 0 and 2, constructed according to (35). One may also construct the effective propagator on the time scale ρ_1^{-1} in accordance with (31, 33): the non-zero matrix elements among sites 0, 1, 2 are

$$G_{01} \simeq e^{\frac{E_{\frac{1}{2}} - F}{2}}, \quad G_{21} \simeq e^{\frac{E_{\frac{3}{2}} - F}{2}}, \quad G_{00} = G_{22} = 1. \quad (42)$$

where the approximate equalities simply indicate that these are propagators under the effective dynamics.

For the next stage of the effective dynamics, the largest hopping rates are r'_0 and ℓ'_2 . Because $E_2 > E_0$, the former will be larger than the latter, and the remaining rates ℓ_0 and r_2 are much smaller by our assumption (40). Correspondingly, when we calculate rates ρ and λ for the next stage of the effective dynamics, the largest one will be $\rho'_0 = \frac{1}{2}(r'_0 + \ell_0 + \ell'_2) + \frac{1}{2}\sqrt{r'^2_0 + 2r_0(\ell'_2 + \ell_0) + (\ell'_2 - \ell_0)^2}$. From the assumptions (40), we have $\ell'_0 \ll \ell_2$, and the rules of the effective dynamics state that we merge sites 0 and 2. Physically, the site energies E_0 and E_2 are similar so these are combined into an effective trap which also contains the intervening site 1. In accordance with (30), the slow degrees of freedom are now simply $\{\dots, p_{012}(t), \dots\}$ where $p_{012}(t) = p_0(t) + p_1(t) + p_2(t)$ is the occupancy of an effective trap containing sites 0, 1 and 2. The corresponding energy landscape is shown in Fig. 3c. The equation of motion for $p_{012}(t)$ at this stage is

$$\partial_t p_{012}(t) = r_{-1}p_{-1}(t) + \ell_3 p_3(t) - (r_{012} + \ell_{012})p_{012}(t) \quad (43)$$

where the new rates appearing at this stage are $r_{012} = e^{-F_{012} - E_{\frac{5}{2}}}$ for hops to the right from the effective trap, and $\ell_{012} = e^{-F_{012} - E_{-\frac{1}{2}}}$ for hops to the left. Here, F_{012} is the trap free energy, $e^{F_{012}} = e^{E_0} + e^{E_1} + e^{E_2}$, in accordance with (32). The approximate propagator on time scales $1/\rho'_0$ can be constructed from (31, 33), giving

$$G_{ji} = e^{E_j - F_{012}}, \quad 0 \leq i, j \leq 2. \quad (44)$$

which is independent of the initial site i as long as it is within the trap, consistent with the idea of local equilibration.

4.3. Comparison with other schemes

It is useful to compare this scheme with the effective dynamics of DMF [12]. In that scheme, the slow degrees of freedom $p_\alpha(t)$ are simply a subset of the original site occupancies $p_i(t)$, so each effective trap contains exactly one site: $a_\alpha = b_\alpha$ for all α . Further, instead of calculating transition state free energies as in (35), one

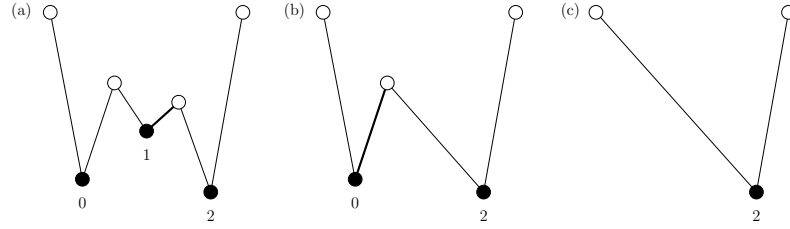


Figure 4. Illustration of the RG scheme of DMF, discussed in the main text. (a) Energy landscape associated with a master operator satisfying (40). The fastest rate r_1 is associated with the energy difference $E_1 + E_{\frac{3}{2}}$: the link associated with this rate is emphasised in bold. (b) Energy landscape associated with the model after one stage of renormalisation using the effective dynamics of DMF. The fast motion on these time scales involves a particle initially on site 1 relaxing onto site 2, with probability unity. The link associated with the largest rate of the resulting master operator is again emphasised. (c) Energy landscape after two stages of renormalisation following DMF. Particles initially on sites 0, 1 or 2 will relax onto site 2.

takes simply $e^{F_{\alpha-\frac{1}{2}}} = \max_{b_{\alpha-1} \leq j < a_{\alpha}} e^{E_{j+\frac{1}{2}}}$, assuming that the transition state free energy of each barrier region is dominated by the largest transition state energy within that region. Finally, one also takes simply $\lambda_{\alpha} = \ell_{\alpha}$ and $\rho_{\alpha} = r_{\alpha}$ when deciding which traps to remove as Γ is reduced. The progress of the scheme is illustrated in Fig. 4 for the same example landscape considered in Fig. 3. The first step of the renormalisation scheme takes place when $\Gamma = r_1$ and the slow degrees of freedom after this step are $\{\dots, p_0(t), p_2(t), \dots\}$ as in our scheme. In the DMF scheme, the equation of motion for these degrees of freedom is of the same form as (41), but the new rates are $r'_0 = e^{-E_{\frac{1}{2}} - E_0}$ and $\ell'_2 = e^{-E_{\frac{1}{2}} - E_2}$ [note that $E_{\frac{1}{2}} > E_{\frac{3}{2}}$, from (40), which sets the transition state free energy]. Further, in the DMF scheme, all elements of the approximate propagator are zero or unity: for times of order $1/r_1$, the non-zero elements of the approximate G_{ij} for $0 \leq j \leq 2$ are

$$G_{00} \simeq G_{21} \simeq G_{22} \simeq 1. \quad (45)$$

which can be compared with (42).

Then, the second stage of the scheme takes place at $\Gamma = r'_0$, after which the slow degrees of freedom are $\{\dots, p_2(t), \dots\}$, and the new rates for motion from the trap containing site 2 are $\ell''_2 = e^{-E_{-\frac{1}{2}} - E_2}$ and $r''_2 = e^{-E_{\frac{3}{2}} - E_2}$. For times of order $1/r'_0$, the non-zero elements of the approximate propagator between sites 0, 1, 2 are

$$G_{20} = G_{21} = G_{22} = 1 \quad (46)$$

which can be compared with (44).

In general then, the DMF scheme gives different results to our scheme, although broad features are similar. In the limit where all rates are well-separated: $r_1 \gg \ell_1 \gg \ell_2 \gg r_0 \gg \ell_0, r_2$, it may be verified that the two schemes coincide. That is the condition in which the DMF scheme is exact, and we conclude that our scheme is also exact in that limit. In fact, our scheme is also exact in the less-restricted limit of well-separated rates given in (40), while the DMF method is inaccurate in that case. The clearest differences between the schemes occur in the propagators. For example, comparing (42) with (45), the DMF scheme ignores the possibility that a particle originally on site 1 may relax onto site 0 at this stage, while such transitions

happen with probability approaching $\frac{1}{2}$ if $r_1 \approx \ell_1$. Additionally, under the same condition $r_1 \approx \ell_1$, the transition rates r'_0 and ℓ'_2 differ between the schemes by a factor close to 2. Compared to DMF, these rates are smaller in our new scheme, reflecting the possibility that a particle that hops from site 0 to site 1 may return to site 0 before visiting site 2. As discussed in [10], factors such as these must be included in effective dynamics schemes in order to obtain the correct scaling behaviour for models where many of the $E_{i+\frac{1}{2}}$ are approximately equal.

We also compare the scheme given here with that of MG [23]. That scheme states the slow co-ordinates at each stage and their equations of motion, although the explicit propagator G_{mn} among the original sites of the model is not given. In fact, for one-dimensional hopping models, the ‘full’ MG scheme reduces to a simplified version of our scheme, in which effective traps are always simply removed from the list of slow degrees of freedom, but traps are never merged. In the language of Sec. 4.1, one always assumes that the landscape has a ‘pure trap’ character. In choosing which traps to remove, one takes the parameters $\lambda_\alpha = \rho_\alpha = r_\alpha + \ell_\alpha$, consistent with that assumption. One may verify that this procedure is exact and coincides with our scheme in the limit where all site energies E_i are well-separated from each other: it is therefore appropriate for systems such as pure trap models. However, the scheme does not preserve the duality of Sec. 2: in particular, while it is appropriate for pure trap models, it fails for their duals, which are pure barrier models.

4.4. Operator representation of effective dynamics

The effective dynamics scheme can be interpreted as a projection of the master operator W onto its slow degrees of freedom. Briefly, any master operator can be diagonalised as $W = -\sum_\lambda |\lambda_R\rangle\lambda\langle\lambda_L|$ and its propagator written as $e^{Wt} = \sum_\lambda |\lambda_R\rangle e^{-\lambda t} \langle\lambda_L|$. Time scales are (globally) well-separated if there is a time t such that all of the exponential factors are either negligibly small or close to unity. For times t with that property, the time evolution operator is well-approximated by a projection operator

$$e^{Wt} \approx \mathcal{P}_{\text{ex}}(t^{-1}) \equiv \sum_{\lambda < t^{-1}} |\lambda_R\rangle\langle\lambda_L|, \quad (47)$$

which can be rearranged into the form $e^{Wt} \approx \sum_\alpha |p_\alpha\rangle\langle q_\alpha|$ where the states $|p_\alpha\rangle$ and $\langle q_\alpha|$ have non-negative elements [25]. For the specific case of hopping models, the states $|p_\alpha\rangle$ indicate the effective traps into which the system relaxes on the time scale t , while the vectors $\langle q_\alpha|$ indicate the probabilities of relaxing into these states.

For the effective dynamics, the key point is that motion on time scales longer than $t = \Gamma^{-1}$ can be well-described by a renormalised master operator $W_{\text{R,ex}}(\Gamma) = \mathcal{P}_{\text{ex}}(\Gamma)W\mathcal{P}_{\text{ex}}(\Gamma)$, since eigenmodes with $\lambda t \gg 1$ that are irrelevant at time t are also irrelevant for all longer times [more precisely, $e^{Wt} = e^{W_{\text{R,ex}}(\Gamma)t} + O(e^{-\Gamma t})$ and the error becomes small for $t \gg \Gamma^{-1}$]. In the effective dynamics a set of effective trap and barrier regions corresponds to an operator $\mathcal{P}(\Gamma)$ that approximates $\mathcal{P}_{\text{ex}}(\Gamma)$. We therefore define the renormalised master operator

$$W_{\text{R}}(\Gamma) = \mathcal{P}(\Gamma)W\mathcal{P}(\Gamma) \quad (48)$$

and we note that a corresponding approximation for the propagator is

$$G_{mn}(\Gamma^{-1}) \simeq \langle m|e^{W_{\text{R}}/\Gamma}|n\rangle \simeq \langle m|\mathcal{P}(\Gamma)|n\rangle \quad (49)$$

For consistency with (36) above, the renormalised master operator should take the form

$$W_R(\Gamma) = \sum_{\alpha} (|P_{\alpha+1}\rangle - |P_{\alpha}\rangle)(r_{\alpha}\langle Q_{\alpha}| - \ell_{\alpha+1}\langle Q_{\alpha+1}|) \quad (50)$$

where $|P_{\alpha}\rangle$ and $\langle Q_{\alpha}|$ are vectors associated with trap α . Thus, the effective dynamics represent a renormalisation scheme in the sense that the operator W_R maintains the same form as the original master operator (3) as the cutoff Γ is reduced. To obtain such a form for W_R , we take

$$\mathcal{P}(\Gamma) = \sum_{\alpha} |P_{\alpha}\rangle\langle Q_{\alpha}| \quad (51)$$

where the $|P_{\alpha}\rangle$ and $\langle Q_{\alpha}|$ are approximations to slow eigenvectors of W . Our scheme as given by Eqs. (30-37) corresponds to the choice

$$\langle i|P_{\alpha}\rangle = e^{E_i - F_{\alpha}} \quad (52)$$

and

$$\langle Q_{\alpha}|i\rangle = \begin{cases} v_i^{(\alpha-\frac{1}{2})}, & b_{\alpha-1} < i < a_{\alpha} \\ 1, & a_{\alpha} \leq i \leq b_{\alpha} \\ 1 - v_i^{(\alpha+\frac{1}{2})}, & b_{\alpha} < i < a_{\alpha+1} \end{cases} \quad (53)$$

In Appendix A, we show that the $|P_{\alpha}\rangle$ and $\langle Q_{\alpha}|$ constructed in this way are indeed good approximations to slow eigenvectors of W , under conditions discussed below.

Thus, the effective equation of motion (36) corresponds in operator notation to the equation $\partial_t |P(t)\rangle = W_R(\Gamma)|P(t)\rangle = \mathcal{P}(\Gamma)W\mathcal{P}(\Gamma)|P(t)\rangle$ and the approximate propagator of (31,33) corresponds to $G_{mn}(\Gamma^{-1}) \simeq \langle m|P(\Gamma)|n\rangle$. The quality of these approximations depends on two considerations. Firstly, the validity of the effective equation of motion (36) depends on the extent to which the projection operator $\mathcal{P}(\Gamma)$ approximates $\mathcal{P}_{\text{ex}}(\Gamma)$. Then, the extent to which the propagator $G_{mn}(\Gamma^{-1})$ coincides with $\langle m|P(\Gamma)|n\rangle$ depends in addition on a separation of time scales, as can be seen from the discussion of (47).

We observe that if $\mathcal{P}(\Gamma) \approx \mathcal{P}_{\text{ex}}(\Gamma)$ at all stages in the scheme then the errors associated with the effective dynamics remain small as Γ is reduced, while large errors arise if $\mathcal{P}(\Gamma)$ becomes different from $\mathcal{P}_{\text{ex}}(\Gamma)$. The conditions under which the operator $\mathcal{P}(\Gamma)$ represents a good approximation to $\mathcal{P}_{\text{ex}}(\Gamma)$ are discussed in Appendix A. Some numerical tests are also given in Sec. 5. We summarise here the analytic results of Appendix A: On long time scales (small Γ) we identify the ‘fastest relevant rates’ ℓ_{α} and r_{α} which are comparable to Γ . For a consistent renormalisation flow, we require that these fast relevant rates are typically much larger than all other relevant rates in their neighbourhood, except that (i) fast relevant rates r_{α} may be comparable either to ℓ_{α} or to $\ell_{\alpha+1}$, and (ii) fast relevant rates ℓ_{α} may be comparable either to r_{α} or to $r_{\alpha-1}$. (The condition of globally well-separated time scales described above is not required: it is sufficient that eigenvalues for motion in the same spatial neighbourhood should be well-separated.)

4.5. Renormalisation and duality

To conclude this section, we discuss duality relations for the effective dynamics, restoring superscripts to distinguish between $W^{(1)}$ and $W^{(1/2)}$. If we renormalise an operator $W^{(1)} = S\bar{S}$ according to our scheme, we arrive at a renormalised model

that can be written in the form $W_R^{(1)} = S_R \bar{S}_R$. The operators S_R and \bar{S}_R have the same form as S and \bar{S} , except that sites i are replaced by effective traps α , transition states by effective barriers, and energies by free energies. An important property of our RG procedure is that if we apply it to the dual master operator $W^{(1/2)} = \bar{S}S$, we find that this renormalises precisely to $W_R^{(1/2)} = \bar{S}_R S_R$. Thus, in addition to the basic requirement that $W_R(\Gamma)$ takes the same form as W , our scheme also obeys the general duality relation under landscape inversion. This is of course desirable, as renormalisation schemes should respect all symmetries of the models of interest.

In the illustrations of Figs. 3 and 4, the duality property follows for both the new scheme and that of DMF, because acting on these illustrations with the inversion operation of Fig. 1 leads to the same renormalisation flows that would be obtained by starting with the dual of the original model.

Mathematically, the duality can be shown as follows. At each stage of the RG flow we have effective trap regions associated with $W_R^{(1)}$, with intervening barrier regions. Assigning integer indices α to the traps, the barriers can be associated with indices $\alpha + \frac{1}{2}$. In $W_R^{(1/2)}$ the regions with integer indices α become effective barriers, while those with indices $\alpha + \frac{1}{2}$ become effective traps. The associated free energies F_α and $F_{\alpha+\frac{1}{2}}$ are the same in both cases. In the dual model $W_R^{(1/2)}$, the rates for hopping to right and left from trap $\alpha - \frac{1}{2}$ are $r_{\alpha-\frac{1}{2}} = \ell_\alpha$ and $\ell_{\alpha-\frac{1}{2}} = r_{\alpha-1}$, consistent with (6). One also easily checks that the rates $\lambda_{\alpha+\frac{1}{2}}$ and $\rho_{\alpha+\frac{1}{2}}$ that are obtained on renormalising $W^{(1/2)}$ are the same as those obtained on renormalising $W^{(1)}$, according to $\rho_{\alpha-\frac{1}{2}} = \lambda_\alpha$ and $\lambda_{\alpha+\frac{1}{2}} = \rho_\alpha$. Thus, supposing that we combine traps α and $\alpha + 1$ in an RG step on the model $W^{(1)}$, we also remove barrier $\alpha + \frac{1}{2}$. In the dual model $W^{(1/2)}$, we remove the trap with index $\alpha + \frac{1}{2}$, which corresponds to combining the barrier regions α and $\alpha + 1$. Finally, it can be verified that the rules for merging and removing traps do preserve the duality between $W_R^{(1)}$ and $W_R^{(1/2)}$.

A brief comment is in order on the construction of S_R and \bar{S}_R . From $W_R^{(1)} = \mathcal{P}^{(1)}W^{(1)}\mathcal{P}^{(1)}$ and $W^{(1)} = S\bar{S}$ one might naively identify $S_R = \mathcal{P}^{(1)}S$, $\bar{S}_R = \bar{S}\mathcal{P}^{(1)}$; but this choice does not satisfy the duality requirement that $W_R^{(1/2)} = \bar{S}_R S_R$. A little thought shows that one requires instead $S_R = \mathcal{P}^{(1)}S\mathcal{P}^{(1/2)}$ and $\bar{S}_R = \mathcal{P}^{(1/2)}\bar{S}\mathcal{P}^{(1)}$. Here $\mathcal{P}^{(1/2)} = \sum_\alpha |P_{\alpha+\frac{1}{2}}\rangle\langle Q_{\alpha+\frac{1}{2}}|$ is the projector onto the effective traps of the dual model, with $|P_{\alpha+\frac{1}{2}}\rangle$ and $\langle Q_{\alpha+\frac{1}{2}}|$ constructed in the obvious manner using the duals of (52) and (53). The operators S_R and \bar{S}_R defined in this way are indeed the effective trap and barrier analogues of (7–10), and the desired dual expressions $W_R^{(1)} = S_R \bar{S}_R$ and $W_R^{(1/2)} = \bar{S}_R S_R$ therefore hold. We note finally that not only the master operators but also the propagators produced by our RG scheme obey the required duality: the propagators are the matrix elements of the projectors $\mathcal{P}^{(1)}$ and $\mathcal{P}^{(1/2)}$, and one verifies by direct calculation that $\langle m|\mathcal{P}^{(1)}(|n\rangle - |n+1\rangle) = \langle n + \frac{1}{2}|\mathcal{P}^{(1/2)}(|m + \frac{1}{2}\rangle - |m - \frac{1}{2}\rangle)$ in accordance with the general duality relation (26).

5. Specific disorder distributions

5.1. Mixed trap-barrier models

The renormalisation scheme that we have discussed can be implemented computationally without undue difficulty. It allows rapid estimation of propagators in

these hopping models, both for fixed disorder and for disorder-averaged properties. We first consider a model obtained by mixing the pure trap and barrier models defined above. In the pure trap model, the transition state energies are $E_{i+\frac{1}{2}} = 0$, while site energies are chosen from an exponential distribution with a mean of μ ; that is, $P(E_i) = (1/\mu)e^{-E_i/\mu}$ with $E_i > 0$. In terms of rates, this implies $\ell_i = r_i = w_i$ with $P(w_i) = (1/\mu)w_i^{(1/\mu)-1}$ for $0 < w_i < 1$. Similarly, pure barrier models have $E_i = 0$ for all sites, and transition state energies are exponentially distributed: that is, $L_i = R_i = w_i$ with the same distribution $P(w_i)$.

We mix these models by taking both site and transition state energies to be exponentially distributed with means μ_T and μ_B respectively. The dynamical scaling of these models therefore depends on the parameters μ_T and μ_B . For the pure barrier model ($\mu_T \rightarrow 0$), sites have half-integer indices and moving a distance r typically requires the crossing of a barrier i whose hopping rate is $w_i = e^{E_{i+\frac{1}{2}}} \sim r^{-\mu_B}$. The rate for actually crossing this barrier is suppressed because the particle is delocalised in an effective trap whose width is of order r . In the language of the effective dynamics, the landscape consists of wide effective traps separated by isolated transition states, and each site i within the trap contributes $e^{E_i} = 1$ to e^{F_α} . The result is that the time taken to move a distance r is $\tau(r) \sim e^{F_\alpha + E_{i+\frac{1}{2}}} \sim r/w_i \sim r^{1+\mu}$. In the pure trap model, the typical time for escaping from sites with large E_i is $1/w_i \sim e^{E_i}$, but the barrier regions on this time scale are typically of width r and their free energies therefore also scale as $e^{F_\alpha + \frac{1}{2}} \sim r$, reflecting the probability of reabsorption in the original trap before arriving at a new one [10]. Thus, the typical relevant time scale is again $\tau(r) \sim r^{1+\mu}$.

We define the dynamical exponent z through the relation $\tau \sim r^z$, and identify

$$z = 1 + \mu_B, \quad \mu_B > 1, \mu_T \rightarrow 0 \quad (54)$$

with an analogous relation if $\mu_T > 1$ and $\mu_B \rightarrow 0$.

In the mixed model, the crucial case distinctions are then whether the μ_B and μ_T are larger or smaller than unity. For example, if $\mu_T < 1$, the average value of e^{E_i} is finite, and the free energies of relevant trap regions scale as $e^{F_i} \sim r$. On the other hand, if $\mu_T > 1$, the site-averaged e^{E_i} is no longer finite, and the sum in (32) is dominated by the largest site within the effective trap. In this case $e^{F_i} \sim r^{\mu_T}$. A similar argument applies for μ_B . Combining these results, we arrive at the dynamic exponent for the mixed model

$$z = \max(1, \mu_B) + \max(1, \mu_T) \quad (55)$$

which reduces to the pure trap case if $\mu_B = 0$ and the pure barrier case if $\mu_T = 0$. Fig. 5 shows numerical results that are consistent with (55). Thus, the effective dynamics provide a natural framework in which to derive this kind of scaling result, although the above predictions for the dynamical exponent could presumably be obtained by other means. We also note that the renormalisation arguments of DMF give $z = \mu_B + \mu_T$ which is the correct result when both μ_B and μ_T are greater than unity. This is consistent with our assertion above that if $\mu_B, \mu_T > 1$ the free energies of effective traps and barriers are typically dominated by single sites, and this is precisely the limit in which the scheme of DMF is valid without approximation. To be precise, it follows from the discussion of Appendix A that our effective dynamics scheme is exact in the limit where either μ_B or μ_T is very large, while the DMF scheme is exact in the limit where both μ_B and μ_T are very large.

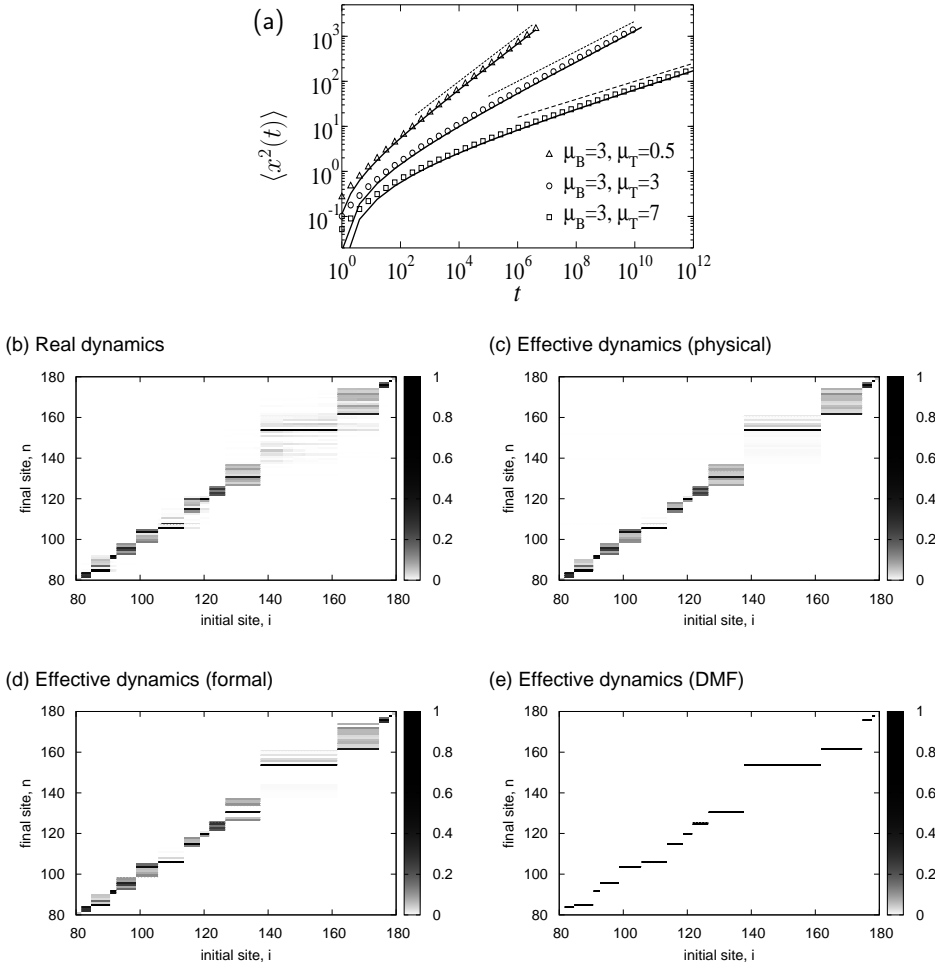


Figure 5. (a) Mean square displacement, showing real dynamics (symbols), effective dynamics (solid lines) and power law predictions of (55) (dashed lines). The DMF scheme (not shown) also gives the correct scaling as long as $\mu_B, \mu_T > 1$ but gives the wrong exponent for the case where $\mu_T = 0.5$. (b,c) Propagators for real dynamics (b) and effective dynamics (c) for the case $\mu_B = 10$ and $\mu_T = 1$. The time is $t = 2^{29}$: the propagator for the real dynamics is obtained by simulating its dual model and using (26), since models with large μ_T can be simulated much more efficiently than those with large μ_B . Since μ_B is large, nearby rates are well-separated and the effective dynamics gives a good approximation to the propagator even for fixed disorder. However, there are deviations in some neighbourhoods which are associated with the presence of eigenvalues of the same order as $1/t$, as discussed in the text. (d,e) Propagators for the formal effective dynamics scheme (see Appendix A) and the DMF scheme (see Sec. 4.2). The formal scheme differs slightly from the physical scheme: for example, the formal scheme gives $G_{ij} = 0$ for $i = 131, 132$, independent of j , while the physical scheme gives small finite values that are more consistent with the real dynamics. In the DMF scheme, all effective traps consist of single sites, so the scheme does not capture the broad ‘effective traps’ that are visible in the real dynamics.

In Fig. 5(b,c), we show example propagators obtained using real and effective dynamics for the case $\mu_B = 10$, $\mu_T = 1$. For these parameters, time scales in a given neighbourhood are sufficiently well-separated that the effective dynamics gives a good approximation to the propagator. In this case, it appears that the largest deviations between real and effective dynamics come from neighbourhoods in which there is an eigenvalue of W of the order of $1/t$. In the discussion of Sec. 4.4, we noted that such deviations are expected even when our scheme gives $P(\Gamma)$ exactly equal to $P_{\text{ex}}(\Gamma)$, and that the specific deviations seen at any time t should decay as time increases, so that the exact and approximate propagators remain close. Our results are consistent with this expectation. For example, comparing Figs. 5b and 5c, the effective dynamics indicates that sites in the vicinity of site 110 are separated into three traps, containing sites 106-113, 114-118, and 119-121: the effective barrier regions are simply single transition states. However, the real dynamics reveals that initial sites 114 – 118 propagate both within that effective trap, and into the adjacent traps. On time scales much shorter than t , one would expect localisation within this trap; on longer time scales the trap will either merge with an adjacent trap, or become incorporated into an effective barrier region. We conclude that we have measured the propagator during this crossover, the details of which are not captured by the effective dynamics.

In Fig. 5(d,e), we compare the physical effective dynamics of 4.1 with the formal scheme of Appendix A and the scheme of DMF. As discussed in Sec. 4.3, the DMF scheme assumes that all effective traps consist of only a single site, so for any initial site i , there is a single final site j such that $G_{ji} = 1$, with $G_{ji} = 0$ for all other final sites. It can be seen that the DMF scheme does identify final sites j with large G_{ji} , but it underestimates G_{ji} for other j . As discussed in Appendix A, our physical effective dynamics scheme means that for a given i , G_{ji} is finite for j within contiguous regions of the chain; on the other hand, the formal scheme leads to G_{ji} that is finite on a restricted set of sites within such regions. As discussed in the caption to Fig. 5, the formal scheme therefore underestimates G_{ji} for some sites j . Since $\mu_B = 10$ is quite large, we expect both of our effective dynamics schemes to mimic the real dynamics quite accurately, consistent with the data. Deviations between the two schemes and the real dynamics would increase as μ_B is reduced (data not shown). Similarly, the predictions of the DMF would mimic the real dynamics more closely if μ_T were increased since that scheme requires both μ_T and μ_B to be large.

Moving to disorder-averaged properties, numerical results indicate that the long-time behaviour in these systems is associated with a scaling form of the diffusion front, as expected. That is (with k the distance between initial and final site as before),

$$\overline{G}_k(t) \approx \sigma^{-1} g(k/\sigma). \quad (56)$$

where the function $g(x)$ is independent of the time t and we use $\sigma = \sigma(t) = 1/\overline{G}_0(t)$ as an estimate of the length scale associated with motion on a time scale t , ensuring that $g(0) = 1$. Our numerical results then indicate that the shape of the diffusion front $g(x)$ depends quite strongly on $\max(\mu_B, \mu_T)$ and much more weakly on $\min(\mu_B, \mu_T)$. As in Ref. [10], the effective dynamics give good agreement with the real dynamics when either μ_B or μ_T is large, with deviations at smaller μ that arise because time scales associated with hopping rates in the same neighbourhood are not well-separated. We show some illustrative results in Fig. 6: the fit for the effective dynamics with $\mu_B = \mu_T = 3$ is strikingly good. However, reducing the value of μ_T further has an effect on the diffusion front for the effective dynamics, while no effect is discernable for the real dynamics. This reduces the quality of the fit in this case. (The results shown

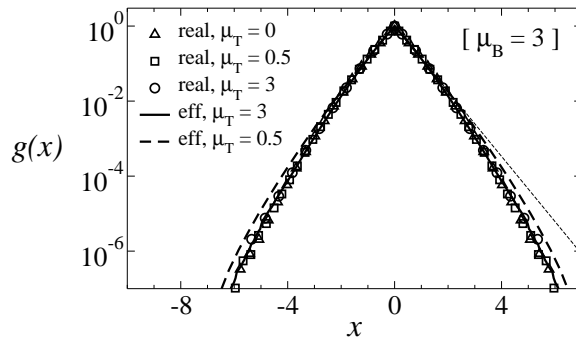


Figure 6. We show estimates of the function $g(x)$ obtained by evaluating $\overline{G}_k(t)$ for times t within the scaling regime. Results are displayed for both real and effective dynamics, with $\mu_B = 3$. Symbols show results for real dynamics with $\mu_T = 0$ (triangles), $\mu_T = 0.5$ (squares) and $\mu_T = 3$ (circles). The times are chosen to lie in the scaling regime and vary from 2^{12} to 2^{24} , according to the model: we note that while the functions $g(x)$ are similar in all cases, the values and scalings of the mean square displacements are different, according to (55). The solid line shows the result for the effective dynamics and $\mu_T = \mu_B = 3$, while the heavy dashed line shows effective dynamics for $\mu_B = 3$, $\mu_T = 0.5$. The light dashed line is a simple exponential distribution. The scheme of DMF (not shown) gives reasonable agreement for $\mu_T = \mu_B = 3$, but this agreement breaks down as μ_T (or μ_B) is reduced.

are for the physical effective dynamics scheme. For these disorder-averaged quantities, we note in passing that the differences between our ‘physical’ and ‘formal’ schemes are of the same order as the differences between real and effective dynamics, with the physical scheme being slightly closer to the real dynamics than the formal one.)

We also find that numerical implementation of the DMF procedure yields reasonable agreement with mean-square displacement and the diffusion front for the case $\mu_B = \mu_T = 3$. However, this agreement breaks down as μ_T is reduced: for $\mu_T < 1$, the DMF scheme yields the wrong dynamical exponent, as discussed above. Thus, the main advantage of the scheme presented here is that it captures the crossover as μ_T gets small [see Eq. (55)]; in this case, it also gives more accurate results for the propagators at fixed disorder (recall Fig. 5(c,d,e)).

Finally, we note that when calculating propagators, we expect the various schemes (DMF, Mon03, that of [10], and the one presented here) to be equivalent in the limit of large μ , at least at the level of the diffusion front. However, the approach to that limit is non-trivial and involves effects that are non-perturbative in μ : the scheme presented here captures some of these effects, which results in improved fits to the diffusion front. In the next section, we illustrate this in the case of the pure trap model. Of course, because of duality, an essentially identical discussion can be given for the pure barrier case.

5.2. Comparison of RG schemes in the pure trap models

We recall that the pure trap model is the case $\mu_B \rightarrow 0$; we then write $\mu_T = \mu$. Applying the DMF method directly to the pure trap model results in a dynamical

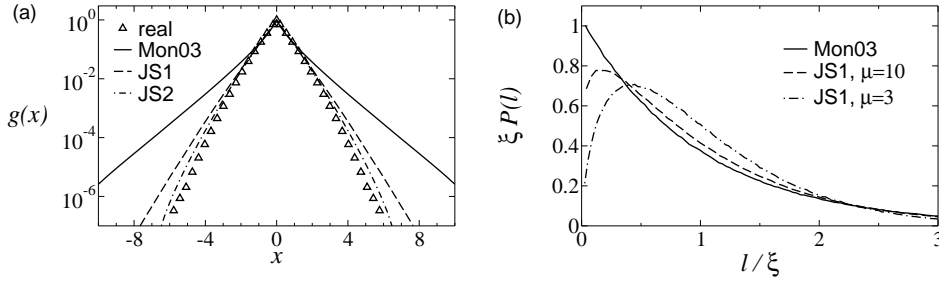


Figure 7. (a) Scaling form for the disorder-averaged diffusion front for the pure trap model with $\mu_T = 3$, $\mu_B = 0$. We show the results for real dynamics and various approximations to this function, obtained by simulations of effective dynamics schemes. All results are taken from the scaling regime, with in particular $t = 2^{17}$ for the real dynamics. We show the Mon03 scheme of Ref. [17], which yields (58); the scheme of [10] (labelled JS1); and the scheme discussed in this article (labelled JS2). (b) Distribution of barrier widths $P(l)$ in the effective dynamics, scaled by its mean ξ . We show results for the effective dynamics scheme of Mon03 in which $P(l)$ is a simple exponential, and two distributions obtained with the scheme JS1.

exponent $z = \mu$. As noted in [17], this result is incorrect: the route taken by Monthus was simply to introduce a factor of the root mean square displacement when converting the rate Γ to a time t . With this change, the dynamical scaling given by the Mon03 scheme [17] is correct.

In Fig. 7, we compare the effective dynamics scheme set out in this article with that of [10] and with Mon03 [17]. The differences are quite striking, as we now discuss. In the schemes of [10] and [17], all effective trap regions are single sites, and the RG scheme relates the propagator to the distribution $P(l)$ of the widths l of effective barrier regions. [We normalise $P(l)$ to $\int_0^\infty dl l P(l) = 1$, such that the probability for a randomly chosen transition state to be in a barrier region of width l is $lP(l)$. Results for $P(l)$ from our current RG scheme are not given here because even for a pure trap model the RG flow eventually leads to a mixture of effective traps and effective barriers which cannot be characterised by a single distribution $P(l)$.] If a given barrier region is delimited by sites b and $b+l$, then the propagator is $G_{n,m} = \delta_{n,b} \frac{b+l-m}{l} + \delta_{n,b+l} \frac{m-b}{l}$ for $b \leq m \leq b+l$. Averaging over all initial sites m at fixed $k = n - m$ on a long chain with the relevant distribution of barrier widths, we arrive at the disorder-averaged diffusion front,

$$\overline{G}_k = \int_{|k|}^{\infty} dl \frac{l - |k|}{l} P(l) \quad (57)$$

where we have assumed that t is large, so that $P(l)$ is smooth, and we may convert sums over l to integrals. Within the Mon03 scheme, the distances l are all independently and identically distributed with an exponential form $P(l) = \xi^{-2} e^{-l/\xi}$. This leads to an estimate for the diffusion front in the limit of large μ :

$$\overline{G}_k \approx \xi^{-1} e^{-k/\xi} \int_0^\infty dy \frac{y}{y + k/\xi} e^{-y} \quad (58)$$

so that the diffusion front is a scaling function of $x = k/\sigma$ for large times, with $\sigma = \xi$. The assumption of Ref. [17] is that, while working at large finite μ does affect $P(l)$, these changes lead to perturbative corrections to the diffusion front.

However, Fig. 7 shows that the tail of the diffusion front is rather different from the prediction (58) of Ref. [17], at least for $\mu = 3$. The effective dynamics scheme discussed in this paper gives more accurate predictions for this tail. In fact, the convergence of the tail of the diffusion front to its large- μ prediction is quite slow. Instead of plotting the diffusion front data directly, we show barrier width distributions $P(l)$ for the effective dynamics schemes of Refs. [17] and [10]. (The distribution $P(l)$ is obtained directly from the effective dynamics: in fact this was the route by which \overline{G}_k was evaluated in Figs. 6 and 7(a).) If we define the mean barrier width to be ξ , then we find that $P(l)$ converges to the simple exponential distribution only if we take $\mu \rightarrow \infty$ at a fixed value of the scaling variable l/ξ . For smaller l there are corrections to this distribution that cannot be accounted for by treating $1/\mu$ perturbatively. Indeed, our numerical results are most consistent with the tail of the diffusion front scaling as

$$\log \overline{G}_k \sim -|k|^{1+\alpha} \quad (59)$$

where $\alpha > 0$ is a power that vanishes as $\mu \rightarrow \infty$. In this case it is clear that the limits of large μ and large k do not commute and hence that working perturbatively in $1/\mu$ is likely to fail when considering the large- k limit of \overline{G}_k . We have not found an analytical treatment which can determine the resulting exponent α , neither exactly nor for our effective dynamics. However, the numerical evidence of Fig. 7 is that our scheme does capture the non-perturbative effects which lead to slow convergence of the diffusion front to the large μ limit.

6. Outlook

In this article, we have derived duality relations that connect pairs of hopping models linked by an inversion of their energy landscape. The simplest case is that of models with equilibrium steady states and periodic boundary conditions, but we were able also to link models with absorbing and reflecting boundary conditions. Somewhat surprisingly, certain periodic systems (pure trap and barrier models with a bias) in which the steady state has a finite current can be analysed similarly [21]. All duality relations are initially expressed in terms of the relevant master operators, but we showed that one can then also construct the propagator of each model from its dual. It follows further that the disorder-averaged propagators in each pair of models are equal on all time and length scales. We discussed an alternative duality relation giving the same results, which is independent of the disorder and related to one used by Schütz and Mussawisade [11] for a reaction-diffusion model.

We have also introduced an effective dynamics scheme for these hopping models. It incorporates both the scheme of Ref. [10] and that of DMF, allowing a broad class of models to be treated in a unified fashion. For a range of “mixed trap-barrier models”, including the pure barrier and trap cases, we have also shown that our scheme captures non-perturbative corrections to the schemes of DMF and Mon03.

Our results also identify a few questions: can explicit expressions for the disorder-averaged diffusion fronts be derived for the mixed model or for the pure trap/barrier cases, either exactly or at least within the effective dynamics? It appears that the diffusion front in the mixed model depends only on the larger of μ_B and μ_T : can this be established? More speculatively, one might ask if the methods used here can be generalised in order to identify effective trap and barrier regions for higher-dimensional systems. We leave these issues for future work.

Acknowledgments

We thank Jean-Philippe Bouchaud, Jeppe Dyre, Jorge Kurchan, Peter Mayer and Cécile Monthus for helpful discussions. We thank Gunter Schütz for bringing Ref. [11] to our attention.

Appendix A. Effective dynamics

In this appendix we give some details of the renormalisation scheme that underlies our effective dynamics. The scheme gives a good description of the dynamics of the model in the limit in which rates in the same neighbourhood are sufficiently well-separated. We first derive the version of the RG procedure that is most natural from a formal point of view, but then argue in favour of the more physically-motivated scheme described in the main text. Both schemes agree in the relevant limit where time scales are locally well-separated, and we argue that the scheme of the main text captures the subleading corrections to this limit more effectively.

Appendix A.1. Formal scheme

Suppose that we have a master operator $W_R(\Gamma)$ of the form given in (50), and that this operator gives an accurate description of motion on time scales longer than Γ^{-1} . We wish to construct a projection operator $P(\Gamma - \delta\Gamma)$ which represents a good approximation to the operator $P_{\text{ex}}(\Gamma - \delta\Gamma)$ of (47), so that $W_R(\Gamma - \delta\Gamma) = P(\Gamma - \delta\Gamma)W_R(\Gamma)P(\Gamma - \delta\Gamma)$ gives an accurate description of motion on time scales longer than $(\Gamma - \delta\Gamma)^{-1}$. In addition, for the scheme to represent a renormalisation group flow, we require that $W_R(\Gamma - \delta\Gamma)$ is also of the form given in (50).

As discussed in the text, we begin by estimating an eigenmode of $W_R(\Gamma)$ that is concerned with fast motion. To achieve this, we imagine that all the rates r_α and ℓ_α are associated with very slow motion, except the triplet $\{r_\alpha, \ell_\alpha, \ell_{\alpha+1}\}$. In that case we can write the master operator as

$$W_R(\Gamma) \approx W_0 = (|P_{\alpha-1}\rangle \quad |P_\alpha\rangle \quad |P_{\alpha+1}\rangle) \begin{pmatrix} 0 & \ell_\alpha & 0 \\ 0 & -(\ell_\alpha + r_\alpha) & \ell_{\alpha+1} \\ 0 & r_\alpha & -\ell_{\alpha+1} \end{pmatrix} \begin{pmatrix} \langle Q_{\alpha-1} | \\ \langle Q_\alpha | \\ \langle Q_{\alpha+1} | \end{pmatrix} \quad (\text{A.1})$$

Diagonalising yields three eigenvalues. Since we have assumed that transitions out of site $\alpha - 1$ are very slow the ‘steady state’, i.e. the right eigenvector with eigenvalue zero, of this reduced system is simply localised on that site. Then there are two negative eigenvalues whose moduli are $\rho_\pm = \frac{1}{2}(r_\alpha + \ell_\alpha + \ell_{\alpha+1}) \pm \frac{1}{2}\sqrt{r_\alpha^2 + 2r_\alpha(\ell_\alpha + \ell_{\alpha+1}) + (\ell_\alpha - \ell_{\alpha+1})^2}$. These eigenvalues are associated with fast (+) and slow (-) motion. We identify ρ_+ as a rate for fast motion to the right from effective trap α . The effective dynamics proceeds by successive removal of the fastest such modes: recall (38), where ρ_+ is written as ρ_α . As discussed in the main text in addition to triplets of rates $(r_\alpha, \ell_\alpha, \ell_{\alpha+1})$, we also consider triplets such as $(\ell_\alpha, r_\alpha, r_{\alpha-1})$, for which the same treatment applies, with the rate λ_α of the fastest mode given in (39). In the discussion below we assume for concreteness that the largest approximate eigenvalue among the $\{\rho_\alpha, \lambda_\alpha\}$ is $\rho_\alpha \equiv \rho_+$.

To accomplish the removal of the fastest mode, we will project the original master operator $W_R(\Gamma)$ onto the basis spanned by the eigenvectors associated with the slow motion. More precisely, the zero eigenvectors of the approximate master operator W_0

are $|P_{\alpha-1}\rangle$ to the right and $\langle e_3| = \langle Q_{\alpha-1}| + \langle Q_\alpha| + \langle Q_{\alpha+1}|$ to the left. The right and left slow eigenvectors, corresponding to eigenvalue ρ_- , we write as $|\rho_-\rangle$ and $\langle\rho_-|$. We therefore define a projection operator whose matrix elements will give the propagator on time scales longer than $1/\rho_+$:

$$\mathcal{P}_+ \equiv \sum_{\alpha'=-\infty}^{\alpha-2} |P_{\alpha'}\rangle\langle Q_{\alpha'}| + |P_{\alpha-1}\rangle\langle e_3| + |\rho_-\rangle\langle\rho_-| + \sum_{\alpha'=\alpha+2}^{\infty} |P_{\alpha'}\rangle\langle Q_{\alpha'}| \quad (\text{A.2})$$

In general, the operator $\mathcal{P}_+W_R(\Gamma)\mathcal{P}_+$ is not of the same form as $W_R(\Gamma)$: it contains hopping processes between next-nearest neighbours for the effective traps, and does not represent a suitable approximation to $W_R(\Gamma - \delta\Gamma)$. This effect is familiar in renormalisation schemes, and requires irrelevant terms in the master equation to be discarded. In our situation, next-nearest neighbour hopping becomes irrelevant as time scales become well-separated. For example, in the barrier-like case where $r_\alpha \approx \ell_{\alpha+1}$ but $r_\alpha \gg \ell_\alpha$, we have

$$\begin{aligned} \mathcal{P}_+ \approx \mathcal{P}_B \equiv & \sum_{\alpha'=-\infty}^{\alpha-2} |P_{\alpha'}\rangle\langle Q_{\alpha'}| + |P_{\alpha-1}\rangle\langle Q_{\alpha-1}| + |P'\rangle(\langle Q_\alpha| + \langle Q_{\alpha+1}|) \\ & + \sum_{\alpha'=\alpha+2}^{\infty} |P_{\alpha'}\rangle\langle Q_{\alpha'}| \end{aligned} \quad (\text{A.3})$$

with

$$|P'\rangle = \frac{\ell_{\alpha+1}}{r_\alpha + \ell_{\alpha+1}}|P_\alpha\rangle + \frac{r_\alpha}{r_\alpha + \ell_{\alpha+1}}|P_{\alpha+1}\rangle. \quad (\text{A.4})$$

We identify $|P'\rangle$ as the right eigenvector associated with a new effective trap that combines traps α and $\alpha + 1$. The resulting master operator $\mathcal{P}_B W_R(\Gamma)\mathcal{P}_B$ is now of the same form as $W_R(\Gamma)$, with the free energy of the new effective trap given by $e^{F_{\alpha,\alpha+1}} = e^{F_\alpha} + e^{F_{\alpha+1}}$. Thus, we may perform an RG step by taking $\mathcal{P}(\Gamma - \delta\Gamma) = \mathcal{P}_B$ as our approximation to $\mathcal{P}_{\text{ex}}(\Gamma - \delta\Gamma)$. Such an RG step is illustrated by the transition between Fig. 3b and Fig. 3c: consistent with that figure, the transition states on either side of the new trap are unchanged during this procedure.

On the other hand, in the trap-like case where $\ell_\alpha \approx r_\alpha$ but $r_\alpha \gg \ell_{\alpha+1}$, we have

$$\begin{aligned} \mathcal{P}_+ \approx \mathcal{P}_T \equiv & \sum_{\alpha'=-\infty}^{\alpha-2} |P_{\alpha'}\rangle\langle Q_{\alpha'}| + |P_{\alpha-1}\rangle(\langle e_3| - \langle Q'|) + |P_{\alpha+1}\rangle\langle Q'| \\ & + \sum_{\alpha'=\alpha+2}^{\infty} |P_{\alpha'}\rangle\langle Q_{\alpha'}| \end{aligned} \quad (\text{A.5})$$

with

$$\langle Q'| = \frac{r_\alpha}{r_\alpha + \ell_\alpha} \langle Q_\alpha| + \langle Q_{\alpha+1}|. \quad (\text{A.6})$$

As for the previous case, $\mathcal{P}_T W_R(\Gamma)\mathcal{P}_T$ is of the same form as $W_R(\Gamma)$, so the choice $\mathcal{P}(\Gamma - \delta\Gamma) = \mathcal{P}_T$ corresponds to a valid RG step. In this step, trap α has been incorporated into a new effective barrier region that merges the old barrier regions $\alpha - \frac{1}{2}$ and $\alpha + \frac{1}{2}$. Its escape properties to the remaining effective traps $\alpha + 1$ and $\alpha - 1$ are described by the eigenvectors $\langle Q'|$ and $\langle e_3| - \langle Q'| = \langle Q_{\alpha-1}| + \ell_\alpha/(r_\alpha + \ell_\alpha)\langle Q_\alpha|$, respectively. An example of such an RG step takes place between Figs. 3a and 3b.

It should be noted that if r_α is much greater than both ℓ_α and $\ell_{\alpha+1}$ then both (A.3) and (A.5) reduce to the case of DMF, which is $|P'\rangle = |P_{\alpha+1}\rangle$ and

$\langle Q' | = \langle Q_\alpha | + \langle Q_{\alpha+1} |$. In practice, for any renormalisation step, we choose either to combine traps by taking $P(\Gamma - \delta\Gamma) = P_B$ or otherwise to combine barriers by taking $P(\Gamma - \delta\Gamma) = P_T$. In either case the resulting $W_R(\Gamma - \delta\Gamma)$ is indeed of the same form as $W_R(\Gamma)$: this ensures that our procedure is a valid renormalisation flow in the space of hopping models.

As discussed in Sec. 4.4, the validity of the renormalisation scheme requires that the projection operator evolves with Γ such that $\mathcal{P}(\Gamma - \delta\Gamma) \approx \mathcal{P}_{\text{ex}}(\Gamma - \delta\Gamma)$. Assuming that we combine traps α and $\alpha + 1$, we should have $\mathcal{P}_B \approx \mathcal{P}_+ \approx \mathcal{P}_{\text{ex}}$. Applying perturbation theory to the fast eigenvectors, we find that corrections are small if $r_\alpha + \ell_{\alpha+1} \gg r_{\alpha-1}, \ell_\alpha, r_{\alpha+1}, \ell_{\alpha+2}$. Similarly, if we combine barriers $\alpha \pm \frac{1}{2}$, we require $\ell_\alpha + r_\alpha \gg \ell_{\alpha-1}, r_{\alpha-1}, \ell_{\alpha+1}, r_{\alpha+1}$. Essentially, if the rate r_α is large at a given stage of the RG (in the sense that $\rho_\alpha > \Gamma - \delta\Gamma$), then r_α must be larger than all rates in the neighbourhood, except for either ℓ_α or $\ell_{\alpha+1}$, one of which may be comparable to r_α .

Appendix A.2. Illustrative example, and comparison with physical scheme of the main text

The formal scheme derived above differs from the one set out in the main text in the way effective traps and barriers are combined. We illustrate this with the system of Fig. 3. The bare master operator is

$$W = \dots + (|0\rangle - |1\rangle)(\ell_1\langle 1| - r_0\langle 0|) + (|1\rangle - |2\rangle)(\ell_2\langle 2| - r_1\langle 1|) + \dots \quad (\text{A.7})$$

where the \dots indicate the remaining terms in the master operator, including those for hopping into and out of this segment of the chain.

Applying the first step of the formal RG scheme, we construct the projection operator

$$\mathcal{P} = \dots + |0\rangle\langle Q_0| + |2\rangle\langle Q_2| + \dots \quad (\text{A.8})$$

where $\langle Q_0| = \langle 0| + e^{\frac{E_1}{2} - F}\langle 1|$ and $\langle Q_2| = \langle 2| + e^{\frac{E_3}{2} - F}\langle 1|$ are constructed according to (A.6), with $e^F = e^{\frac{E_1}{2}} + e^{\frac{E_3}{2}}$. This leads to the same result as the physical scheme of the text, since (A.8) is also consistent with (53) above. The renormalised master operator is

$$W_R = \mathcal{P}W\mathcal{P} = \dots + (|0\rangle - |2\rangle)e^{-F}(e^{-E_2}\langle Q_2| - e^{-E_0}\langle Q_0|) + \dots \quad (\text{A.9})$$

Applying the formal scheme again to this operator, the projection operator is

$$\begin{aligned} \mathcal{P}' &= \dots + |P_{02}\rangle(\langle Q_0| + \langle Q_2|) + \dots \\ &= \dots + |P_{02}\rangle(\langle 0| + \langle 1| + \langle 2|) + \dots \end{aligned} \quad (\text{A.10})$$

where $|P_{02}\rangle = e^{-F_{02}}(e^{E_0}|0\rangle + e^{E_2}|2\rangle)$ with $e^{F_{02}} = e^{E_0} + e^{E_2}$. According to the scheme of the main text, we would have obtained a similar result, but with the replacement $|P_{02}\rangle \rightarrow |P_{012}\rangle = e^{-F_{012}}(e^{E_0}|0\rangle + e^{E_1}|1\rangle + e^{E_2}|2\rangle)$, where $e^{F_{012}} = e^{E_0} + e^{E_1} + e^{E_2}$.

In the limit where rates are well-separated and the formal scheme is exact, it follows from (40) that $E_1 \ll E_0, E_2$, and in this case, the physical and formal schemes coincide. Indeed, it may be shown that the errors associated with the physical and formal schemes are of the same order. We conclude that the physical scheme is at least as appropriate as the formal one and indeed it can be verified that the errors are of the same order.

The key point is that the physical scheme of the text is based on the assumption of equilibration within effective traps. Under that assumption, it is clear that the

states $|P_\alpha\rangle$ should coincide with Boltzmann distributions over the sites within the trap. In general, the formal scheme gives a state $|P_\alpha\rangle$ that is finite only on a subset of the sites within the trap. This is a necessary feature of the formal scheme, because the $|P_\alpha\rangle$ at each stage are constructed from the $|P_\alpha\rangle$ of the previous stage. In the language of section 4.1, the slow co-ordinates $p_\alpha(t)$ must be linear combinations of the p_α of the previous stage. Thus, since site 1 in the example of Fig. 3 is not contained in any of the p_α after the first step of the RG, it can never be part of an effective trap at any future stage. Equivalently, the $|P_\alpha\rangle$ can have no contribution from site 1 in future stages, and may not correspond to Boltzmann distributions of the whole trap. This in turn means that the approximate propagator $\langle n|\mathcal{P}(\Gamma)|m\rangle$ is equal to zero for some final sites n within effective traps, underestimating the true value of $G_{nm}(\Gamma^{-1})$ there. The differences between the formal and physical schemes are shown numerically in Fig. 5, which illustrates how the formal scheme underestimates the probability of propagation onto certain sites within the effective traps, for specific disorder realisations. As discussed in Sec. 5, the physical and formal schemes show differences in the tails of the disorder-averaged diffusion front that are of the same order as the deviations between real and effective dynamics.

Finally, we note that the physical scheme is not strictly a renormalisation flow in that the rates and free energies at a given stage, depend not just on the renormalised operator W_R at the previous stage, but on all the bare energies E_i and $E_{i+\frac{1}{2}}$. If this feature is considered undesirable, the formal scheme may be used. However, the interpretation of the physical scheme as a partition into contiguous trap and barrier regions and the intuitive idea of equilibration within effective trap regions means that we prefer that route.

References

- [1] M. D. Ediger, *Annu. Rev. Phys. Chem.* **51**, 99 (2000); E. R. Weeks *et al.*, *Science* **287**, 627 (2000); W. Kegel and A. van Blaaderen, *Science* **287**, 290 (2000).
- [2] M. T. Cicerone, P. A. Wagner, and M. D. Ediger, *J. Phys. Chem. B* **101**, 8727 (1997); R. Yamamoto and A. Onuki, *Phys. Rev. Lett.* **81**, 4915 (1998); C. Donati *et al.*, *Phys. Rev. E* **60**, 3107 (1999); B. Doliwa and A. Heuer, *Phys. Rev. E* **67**, 030501 (2003); Y. Jung, J. P. Garrahan and D. Chandler, *Phys. Rev. E* **69**, 061205 (2004).
- [3] See, for example, M. J. Saxton and K. Jacobson, *Annu. Rev. Biophys. Biomol. Struct.* **26**, 373 (1997); M. Weiss *et al.*, *Biophys. J.* **87**, 3518 (2004); D. S. Banks and C. Fradin, *Biophys. J.* **89**, 2960 (2005); I. Golding and E. Cox, *Phys. Rev. Lett.* **96**, 098102 (2006); M. A. Lomholt, I. M. Zaid and R. Metzler, *Phys. Rev. Lett.* **98**, 200603 (2006).
- [4] J. Bernasconi *et al.*, *Phys. Rev. Lett.* **42**, 819 (1979).
- [5] E. Bertin, J.-P. Bouchaud and F. Lequeux, *Phys. Rev. Lett.* **95**, 015702 (2005); R. L. Jack, P. Sollich and P. Mayer, *Phys. Rev. E* **78**, 061107 (2008).
- [6] S. Alexander *et al.*, *Rev. Mod. Phys.* **53**, 175 (1981).
- [7] S. Havlin and D. Ben Avraham, *Adv. Phys.* **36**, 695 (1987).
- [8] J.-P. Bouchaud and A. Georges, *Phys Rep* **195**, 127 (1990).
- [9] R. Metzler and J. Klafter, *Phys. Rep.* **339**, 1, (2000).
- [10] R. L. Jack and P. Sollich, *J. Phys. A* **41**, 324001 (2008).
- [11] G. M. Schütz, *Z. Phys. B* **104**, 583 (1997); G. M. Schütz and K. Mussawisade, *Phys. Rev. E* **57**, 2564 (1998).
- [12] P. le Doussal, C. Monthus and D. S. Fisher, *Phys. Rev. E* **59**, 4795 (1999).
- [13] See, for example, D. J. Wales, M. A. Miller and T. R. Walsh, *Nature* **394**, 758 (1998); F. Stillinger, *Science* **267**, 1935 (1995).
- [14] J. Machta, *J. Phys. A* **18**, L531 (1985)
- [15] C. Monthus and J.-P. Bouchaud, *J. Phys. A* **29**, 3847 (1996).
- [16] E. Bertin and J.-P. Bouchaud, *Phys. Rev. E* **67**, 026128 (2003).
- [17] C. Monthus, *Phys. Rev. E* **68**, 036114 (2003).

- [18] S. Tanase-Nicola and J. Kurchan, Phys. Rev. Lett. **91**, 188302 (2003); S. Tanase-Nicola and J. Kurchan, J. Stat. Phys. **116**, 1201 (2004).
- [19] J. Zinn-Justin, *Quantum Field Theory and Critical Phenomena*, chapter 17 (Oxford University Press, Oxford, 2002)
- [20] J. Tailleur, J. Kurchan and V. Lecomte, J. Phys. A **41**, 505001 (2008).
- [21] P. Sollich and R. L. Jack, Prog. Theor. Phys. Supp., in press; see also arXiv:0911.0208.
- [22] P. J. H. Denteneer and M. H. Ernst, Phys. Rev. B **29**, 1755 (1984).
- [23] C. Monthus and T. Garel, J. Phys. A **41**, 255002 (2008); C. Monthus and T. Garel, J. Phys. A **41**, 375005 (2008).
- [24] Y. G. Sinai, Theor. Prob. Appl. **27**, 256 (1983).
- [25] B. Gaveau and L. S. Schulman, J. Math. Phys. **39**, 1517 (1998); see also G. Biroli and J. Kurchan, Phys. Rev. E **64**, 016101 (2001); A. Bovier *et al.*, Commun. Math. Phys. **228**, 219 (2002).